UPPSALA
UNIVERSITET

Digital Comprehensive Summaries of Uppsala Dissertations from the Faculty of Science and Technology 1015

Diamond Microfabrication for Applications in Optics and Chemical Sensing

PONTUS FORSBERG

ACTA
UNIVERSITATIS
UPSALIENSIS
UPPSALA
2013

ISSN 1651-6214
ISBN 978-91-554-8587-0
urn:nbn:se:uu:diva-192567

Dissertation presented at Uppsala University to be publicly examined in Polacksbacken 2347, Lägerhyddsvägen 2, Uppsala, Friday, March 8, 2013 at 10:00 for the degree of Doctor of Philosophy. The examination will be conducted in English.

Abstract
Forsberg, P. 2013. Diamond Microfabrication for Applications in Optics and Chemical Sensing. Acta Universitatis Upsaliensis. *Digital Comprehensive Summaries of Uppsala Dissertations from the Faculty of Science and Technology* 1015. 65 pp. Uppsala.
ISBN 978-91-554-8587-0.

Diamond is a material with many exceptional properties. In this thesis methods for fabrication of microstructures as well as several applications of such structures in optics, microfluidics and electrochemistry are presented.

A method for etching deep and highly precise gratings is described. This method was used to fabricate circularly symmetric half wave plates for use in vector vortex coronagraphs. Such coronagraphs are a very promising approach to the direct imaging of extrasolar planets.

By varying the lateral etch rate of the aluminum mask during diamond etching in an inductively coupled plasma, the sidewall angle of the etched structures could be controlled. This method was used to make smooth sloped sides on a waveguide for coupling light into it. Antireflective structures that drastically reduced the surface reflection in a wavelength band between 10 and 50 μm were also fabricated.

An array of boron doped diamond microelectrodes for electrochemical measurements in a microchannel was fabricated and tested, showing very good stability and reusability. Several hundred hours of use did not adversely affect their performance and no damage to them could be detected by atomic force microscopy or scanning electron microscopy.

Superhydrophobic surfaces in diamond were demonstrated, using both hydrogen and fluorine termination. Hydrogen termination on a flat surface gives contact angles below 90°. To achieve a superhydrophobic surface with this low intrinsic hydrophobicity, structures looking like microscopic nail heads were fabricated. The effect of water pressure on immersed superhydrophobic surfaces was also studied and it was found that the collapse of the superhydrophobic state due to pressure was sometimes reversible as the pressure was lowered.

Finally, a method was tested for functionalizing diamond surfaces using block copolymers of polyethylene oxide and polypropylene oxide to both passivate the surface and to attach synthetic binder molecules. This method was found to give very high signal to noise ratios when detecting C-reactive protein.

Keywords: diamond, microfabrication, microoptics, coronagraph, waveguide, microelectrodes, superhydrophobic

Pontus Forsberg, Uppsala University, Department of Engineering Sciences, Microsystems Technology, 516, SE-751 20 Uppsala, Sweden.

ISSN 1651-6214
ISBN 978-91-554-8587-0
urn:nbn:se:uu:diva-192567 (http://urn.kb.se/resolve?urn=urn:nbn:se:uu:diva-192567)

List of Papers

This thesis is based on the following papers, which are referred to in the text by their Roman numerals.

I P. Forsberg and M. Karlsson, "High aspect ratio optical gratings in diamond," accepted for publication in *Diamond and Related Materials*, January 2013, DOI: 10.1016/j.diamond.2013.01.009.

II C. Delacroix, P. Forsberg, M. Karlsson, D. Mawet, O. Absil, C. Hanot, J. Surdej and S. Habraken, "Design, manufacturing, and performance analysis of mid-infrared achromatic half-wave plates with diamond subwavelength gratings," *Applied Optics* 51 (2012), 5897-5902.

III C. Delacroix, O. Absil, P. Forsberg, D. Mawet, V. Christiaens, M. Karlsson, A. Boccaletti, P. Baudoz, M. Kuittinen, I. Vartianen, J. Surdej and S. Habraken, "Laboratory demonstration of a mid-infrared AGPM vector vortex coronagraph," submitted to *Astronomy and Astrophysics*, January 2013.

IV P. Forsberg and M. Karlsson, "Inclined surfaces in diamond: broadband antireflective structures and coupling light through waveguides," *Optics Express* 21 (2013), 2693-2700.

V K. Fromell, P. Forsberg, M. Karlsson, K. Larsson, F. Nikolajeff and L. Baltzer, "Designed protein binders in combination with nanocrystalline diamond for use in high-sensitivity biosensors," *Analytical and Bioanalytical Chemistry* 404 (2012), 1643-1651.

VI M. Karlsson, P. Forsberg and F. Nikolajeff, "From Hydrophilic to Superhydrophobic: Fabrication of Micrometer-Sized Nail-Head-Shaped Pillars in Diamond," *Langmuir* 26 (2010), 889-893.

VII P. Forsberg, F. Nikolajeff and M. Karlsson, "Cassie-Wenzel and Wenzel-Cassie transitions on immersed superhydrophobic surfaces under hydrostatic pressure," *Soft Matter* 7 (2011), 104-109.

VIII P. Forsberg, E. O. Jorge, L. Nyholm, F. Nikolajeff, M. Karlsson, "Fabrication of boron doped diamond microband electrodes for electrochemical detection in a microfluidic channel," *Diamond and Related Materials* 20 (2011), 1121-1124.

Reprints were made with permission from the respective publishers.

Author's Contribution to the Publications

Paper I	Most of planning, experimental work, evaluation and writing.
Paper II	Part of planning and simulations, most experimental work, part of evaluation and writing.
Paper III	Part of planning, experimental work, evaluation and writing.
Paper IV	Most of planning, experimental work, evaluation and writing.
Paper V	Part of planning, experimental work, evaluation and writing.
Paper VI	Part of planning, experimental work, evaluation and writing.
Paper VII	Most of planning, experimental work, evaluation and writing.
Paper VIII	Part of planning, major part of experimental work, evaluation and writing.

Contents

Abbreviations

AFM	Atomic Force Microscopy
AGPM	Annular Groove Phase Mask
ATR	Attenuated Total Reflectance
CRP	C-Reactive Protein
CVD	Chemical Vapor Deposition
E-beam	Electron beam
HPHT	High Pressure High Temperature
ICP	Inductively Coupled Plasma
IR	Infra Red
MCD	MicroCrystalline Diamond
NCD	NanoCrystalline Diamond
PDMS	PolyDiMethylSiloxane
RCWA	Rigorous Coupled Wave Analysis
RF	Radio Frequency
SEM	Scanning Electron Microscopy
UV	Ultra Violet
VLT	Very Large Telescope
VVC	Vector Vortex Coronagraph

Introduction

Diamond microfabrication. Producing exceedingly fine and precise structures in the hardest material known to man may seem like an impossible task, worthy of some storybook hero. Using modern technology, inherited from the microelectronics industry, it can however be done and it is the subject of this thesis along with some applications of such structures.

The thesis is written around eight papers published in or submitted to academic journals. These can be found appended at the back of this book. They are ordered not chronologically, but simply to facilitate a coherent narrative. The text of the thesis itself is intended as an introduction to and summary of these papers.

The first two sections after this Introduction will provide the reader with some basic understanding of diamond as a material and the tools and methods of microfabrication. Readers who already have a good grasp of these basics may want to skip over one or both of these sections. The section about diamond etching is where we get to the meat of the thesis. Good control of diamond etching is vital for the optical applications presented in the following two sections about sub-wavelength gratings and waveguides. In the section about spectroscopy on diamond waveguides we also get into the importance of controlling the chemistry of a diamond surface, something that is continued in the section about controlling the wettability of diamond surfaces. Finally there is a short section about diamond microelectrodes before the thesis ends with some concluding remarks and, of course, acknowledgements of all the people who have helped me on the long road to this thesis.

Diamond in brief

Diamond. The word brings to mind images of brilliant cut, clear gemstones set in engagement rings and crown jewels. As a researcher it can be rewarding to work with a material that so many people find fascinating. “I work with diamonds” is a great conversation starter if nothing else. Of course, the fascination usually has little to do with the actually remarkable properties of diamond and a lot to do with the fantastically successful marketing campaigns by De Beers in the 20th century [1]. This section will try to give an overview of this in many ways extreme material. We will start with sorting out what diamond is and how it behaves and then briefly cover where the world gets its diamonds from and what they are used for or potentially useful for. The weight of diamonds is often given in carats (1 ct = 0.2 g), but to avoid confusion metric units of mass will be used throughout this thesis.

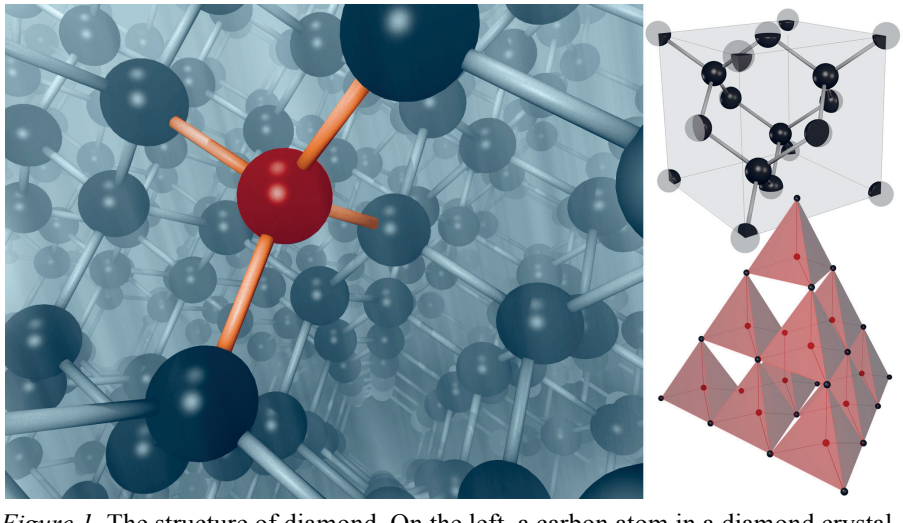

Figure 1. The structure of diamond. On the left, a carbon atom in a diamond crystal with its four strong covalent bonds emphasized (view roughly from the 110 direction). The bond length is around 1.54 Å. On the right, the arrangement of atoms in a unit cell of the diamond crystal structure and the structure described as a stack of tetrahedrons.

Structure

The atoms in a diamond crystal are arranged so that every atom has four closest neighbors with equal angles between them, so that these neighbors sit at the points of a regular tetrahedron. The carbon atom is bound to these neighbors by strong sp^3-hybrid covalent bonds. The crystal structure can be built up by stacking such tetrahedra, as shown in *Figure 1*. This leads to a face centered cubic crystal lattice, with each tetrahedron having one vertex at a corner of the cube and the other three vertices at the center of the faces coming together at that corner. This structure is called a diamond structure and crystals of many other elements share it, such as silicon and germanium. It is this structure in combination with the small size of carbon atoms (which gives a high density of very strong bonds) which gives diamond many of its superlative properties. It should be noted that the covalent bonds in diamond are actually weaker than the sp^2 bonds in graphite (or graphene), but graphite is only covalently bonded in flat sheets with weak forces holding the sheets together, while diamond has a fully covalently bonded three-dimensional structure.

Properties

When asked what they know about diamonds, four things come to mind for many people: they are expensive, the rich and famous like to be seen wearing them, they glitter prettily and they are hard. Diamond is an extraordinary material, but to an engineer what makes it extraordinary is not the diamond ring given to Grace Kelly by Prince Rainier of Monaco or the estimated $5 million worth of diamonds worn by Halle Berry for the 60th Golden Globe awards. Even the price is not very interesting, although it does constrain the range of suitable applications. The way diamonds can catch the light and their hardness, however, are interesting. As are several other, less well known properties.

That diamond can be made to glitter so prettily hints at interesting optical properties. Diamond has a very high refractive index as well as a high optical dispersion (the variation of refractive index with wavelength). The high refractive index also leads to a high reflectance of diamond surfaces. Diamond is transparent over a very wide range of wavelengths from the ultraviolet and up through the infrared and beyond. Further, the ability of so-called nitrogen vacancy centers in diamond to work as single photon sources, has received a lot of attention in recent years [2].

The hardness too is an interesting property, as diamond is the hardest, most incompressible material around. Harder materials have been suggested [3], but have yet to be synthesized in sufficient quantity or purity to test this experimentally. Some polycrystalline composites of diamond have also

shown higher hardness, and perhaps more importantly higher toughness, than single crystal diamond [4, 5]. Hardness represents the resistance to scratching and wear while toughness has to do with resistance to breaking or shattering.

Beyond the optical and mechanical properties, diamond also shows some remarkable thermal, electronic and chemical characteristics. It has the highest thermal conductivity of any known material, five times better than that of copper (a very good thermal conductor) at room temperature or better still for isotopically purer specimens [6]. This is even more remarkable considering pure diamond is a good electrical insulator, while most other good thermal conductors also conduct electricity. Diamond also has a very low thermal expansion. Being pure carbon, diamond will however oxidize at high temperature in the presence of oxygen [7]. At higher temperatures still, with no oxygen present, diamond may turn into graphite, which is the thermodynamically more stable form except at extreme pressures.

Diamond has a wide bandgap and is normally a good insulator, but with proper doping by boron (p-type doping) or phosphorus (n-type) during growth, it can be made semiconducting. With very high levels of boron doping, diamond even shows metallic conduction behavior.

Chemically, diamond is very inert; it doesn't react with most chemicals, be they acids, bases or solvents. Diamond surfaces can however be terminated and functionalized in various ways ([8] and **papers V and VI**), so that interesting chemistry may take place on the diamond surface even though the material itself doesn't react. In electrochemistry, boron doped diamond electrodes show a very wide potential window in water (the potential range in which they do not reduce or oxidize water) (see **paper VIII**).

Sources

Natural diamonds

Most natural diamonds (and all natural gem diamonds) found on the surface of the Earth were formed deep in the planet's mantle under very high pressure and temperature over millions of years, and made their way to the surface during deep volcanic eruptions [9]. Diamonds may also form on the surface of the Earth, but the temperatures and pressures required only occur naturally during meteor impacts. Impact diamonds are polycrystalline aggregates and can be found, sometimes in large quantities, at impact sites with graphite-bearing rocks [10]. Some meteorites also carry diamonds of extraterrestrial origin to Earth. These are typically just a few nanometers in size and may be older than our solar system [11]. There are also macroscopic (and in some cases very large) polycrystalline aggregates called *carbonado,* which may have formed in space [12], although both impact and mantle

origins have been suggested [5]. For mining, the single crystal diamonds formed in the mantle are of most interest. In total, the yearly production of natural diamond is some 30 tonnes, with 95% coming from the seven leading producers: Russia, Botswana, Congo, Angola, Canada, Australia and South Africa [13]. Worldwide there are around 20 major diamond mines [1].

Man-made diamonds

For the past six decades it has been possible to produce diamond synthetically. Synthetic diamond can be produced with any quality, from nanometer sized grains full of defects up to flawless centimeter sized crystals. The possibility to tailor the properties to the application, the lower price and the sheer volumes that can be produced has led to the production of synthetic diamond far outpacing that of natural. Some 880 tonnes are produced annually, nearly 30 times more than natural diamond [14].

Two methods are used to produce macroscopic diamonds: One applying the high pressure and high temperature under which diamond is thermodynamically stable, the other carefully controlling the kinetics while depositing carbon from gas at low pressure. In the high pressure, high temperature (HPHT) approach, graphite is dissolved in a molten metal and allowed to crystallize as diamond. In the low pressure approach, chemical vapor deposition (CVD), diamond is grown in a vacuum chamber containing hydrogen and carbon (typically added in the form of methane) in the gas phase. HPHT is the preferred method for production of diamond material on an industrial scale. The simplicity and versatility of CVD equipment, on the other hand, makes it ideal for research. CVD also allows for finer control of impurities and can be used to produce diamond films over large areas, so it is the method of choice for many high tech applications. A third method used to produce diamond on an industrial scale is the contained detonation of carbon containing explosives. The temperature and pressure during the explosion are high enough for diamond to form. The diamonds formed by this method are typically around 5 nm in size [15].

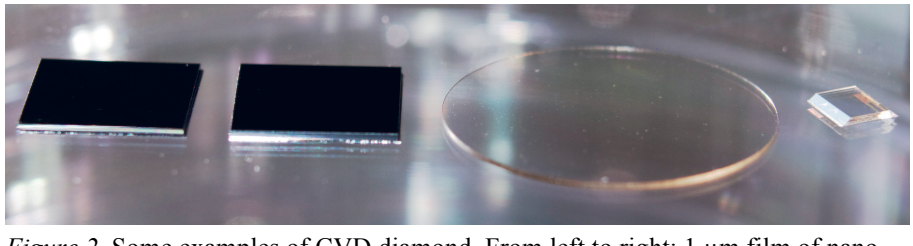

Figure 2. Some examples of CVD diamond. From left to right: 1 µm film of nanocrystalline diamond on silicon; 0.5 µm of boron doped nanocrystalline diamond on silicon; 2 cm diameter, 300 µm thick disk of microcrystalline diamond of optical quality; single crystal diamond prism.

CVD diamond

All diamond material used for the works in this thesis was produced by CVD processes, so a short introduction is in order. CVD comes in many varieties, such as hot filament CVD or magnetron plasma CVD. Common to most of them are high temperatures (2000 K or more in the gas and around 1000 K on the substrate) and a gas phase consisting of hydrogen with a few per cent of carbon. By supplying energy in the form of plasma or heat, reactive species of the gases are formed. These can then react with a surface and slowly build up a diamond crystal. Other carbon materials can also form but, by tuning the system, they can be etched away by the hydrogen. Small amounts of other gases can be added to dope the diamond and/or change the growth rate or morphology. The substrate also plays a crucial role in the growth. Polycrystalline diamond films can be grown on substrates made from a range of carbide forming materials and materials with low carbon diffusion rates including silicon, tungsten, molybdenum, and titanium, although pre-treatments are often necessary for dense and homogeneous nucleation of diamond crystals. Diamond grains grow from nucleation sites on the substrate and increase in size with film thickness. Grains with faster growing crystal directions facing the gas can outcompete surrounding grains. This leads to films of elongated grains that are narrow on the nucleation side and wider on the other. To achieve flat, freestanding polycrystalline diamond plates, the substrate is removed and the rough top side polished. Often the nucleation side is also polished to remove the initial growth layer. Single crystal diamond is typically formed by homoepitaxial growth. Meaning that a diamond substrate of similar lateral dimensions is needed to grow it, which limits the size of single crystal diamond films. Single crystal diamond has been successfully grown on non-diamond substrates, but not without significant defects. Going towards the other extreme, opposite from single crystal diamond, nanocrystalline diamond films with grain sizes between 5 and 100 nm can be grown as very thin, dense films with very low surface roughness. Such films can be formed either by making the nucleation density high enough and the film thickness low enough that large grains cannot form, or by allowing re-nucleation of diamond grains during growth, by for example increasing methane concentration or replacing hydrogen with argon. For a general review of single and polycrystalline CVD diamond see [16] and for nanocrystalline CVD diamond see [17].

Applications

As can be understood from the long list of extraordinary properties, diamond can be useful in an even longer list of applications. Of natural diamonds, more than half still goes to jewelry while the rest goes to industrial uses. Of

the man made diamond production, nearly all is used for industrial applications with only a tiny fraction sold as gemstones. In total more than 98% of all diamond goes to industrial uses [14]. Due to its hardness, diamond is used for applications in cutting, drilling, grinding, polishing and wire drawing; where it can cut faster and last longer than other materials. Tool lifetimes can be increased by as much as a factor 50 [14]. Increased tool life leads to lower costs of tools, but also fewer tool changes and longer production runs. Around 95% of industrial diamond is used for these abrasive applications.

The high thermal conductivity of diamond also makes it an ideal material for heat sinks in electronics and, together with its high transparency in the visible and infrared, for lenses and windows for high-powered lasers [18]. The strength and chemical stability means diamond also finds uses as windows that can resist corrosive atmospheres and high pressures, for wavelengths from the mid ultraviolet up to microwaves (for example between a gyrotron and a fusion reactor). As a wide bandgap semiconductor, diamond can be used for high temperature, high power and high frequency electronics, ultraviolet light emitting diodes and sensors in harsh environments. Boron doped diamond is used as an exceptionally durable electrode material in electrochemical water treatment and its wide potential window in water allows for electrochemical measurements that are not practical with gold or platinum electrodes. Biocompatibility and the possibility to modify the surface chemistry make diamond a promising material in biosensors. The same properties also mean nanodiamonds can be used as carriers to improve the efficacy of cancer medicines [19]. Light emission from nitrogen vacancy centers allow diamond to be used as fluorescence labels in biology and their use as single photon emitters may allow new photonic and quantum mechanical information handling [20].

The studies in this thesis aim to explore and extend the long list of applications for this remarkable material.

Microfabrication

This section aims to give a brief overview of general principles and processes commonly used for making very small things, with some emphasis on those used for the papers in this thesis. The basics I wish to cover are common to many disciplines. Be it microelectronics, microoptics, microfluidics, micromechanics or microelectromechanical systems, if it starts with a "micro-" it likely shares the fabrication basics regardless of the application. I think some basic understanding of these is something everybody should have, as so much of our society is already based on microelectronics (although much of it can rightly be called nanoelectronics these days) and we are starting to take many other microsystems for granted.

We will first look at a basic example of how the process flow can look for etching a pattern into a substrate. Once we have that basic processing idea firmly in mind we will be able to appreciate one of the true strengths of microfabrication: batch processing. After that will follow a slightly more in depth look at some processing methods and materials of interest for this thesis.

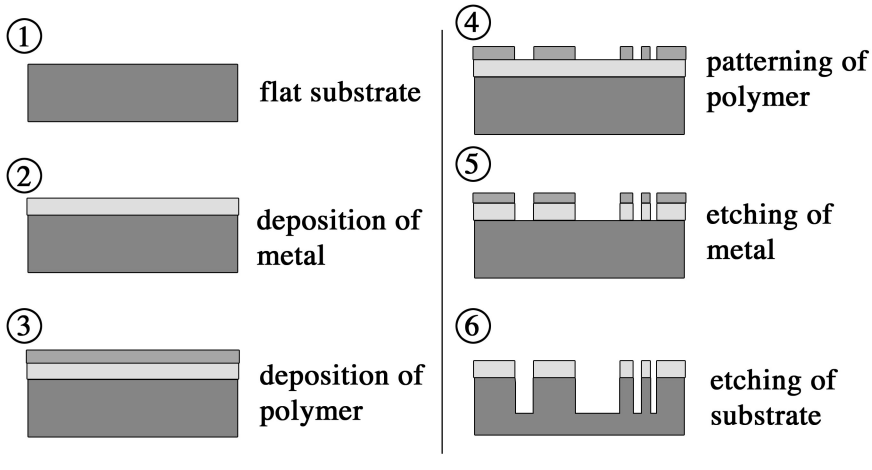

Figure 3. Side view of a basic process flow for etching a pattern in a substrate.

A typical process flow

The process steps in microfabrication are in principle simple and easy to follow. Most of the complexity comes with the practical processing methods and keeping them compatible with one another and the intended use of the fabricated component. Typical basic processing steps are deposition, patterning and etching. There are certainly more, but these three are enough to get pretty far, especially if repeated several times. *Figure 3* shows a simple process where these three steps are used to etch a pattern into a substrate.

One starts with a flat substrate, this can be a silicon wafer but in this thesis it will usually be a diamond piece or silicon with a film of diamond on top. On this substrate a film is deposited, metal is often convenient, but it can also be other materials such as silicon oxide. The important thing is that during the final etching step (6 in *Figure 3*) the mask is etched much slower than the substrate. Next, a polymer film is deposited on top of the metal film. Often this is a photosensitive polymer, which can be patterned by shining light on some parts and not on others (photolithography), but other ways of patterning are also possible. Once the polymer is patterned, the metal is etched. This can be by wet etching in some chemical bath or by dry etching in a reactive plasma. In either case, the metal is only etched away where it is not covered by polymer so that the same pattern that was made in the polymer is now in the metal layer. We can now finally etch the substrate material with the metal mask protecting some areas. With the right choice and thickness of the metal mask, the substrate can now be etched fairly deep; in some cases all the way through. If one had instead wanted a pattern of metal on the substrate, for electrical conductors for example, the process could be ended after step 5 and the remaining polymer dissolved in acetone.

For simple structures, the processing might be done after etching the substrate once and removing the remaining metal film. Other applications may require many cycles of depositing, patterning and etching.

Batch processing

It is important to understand that in each processing step in the above example the entire surface of the substrate is treated at the same time. One does not deposit material only where it is wanted. Material is deposited over the whole surface and then selectively removed. In the patterning step a pattern is transferred lithographically (see below) from a premade template (a shadow mask or a stamp). This template usually has to be made serially, which can be time consuming and expensive, but it can then be used many times. The beauty of this kind of processing is that the size and intricacy of the pattern does not change the time it takes to manufacture, and the number of components that can be produced at once is only limited by how many can

be crammed onto the same substrate. This might not sound too revolutionary until one realizes that it is the basis of the entire digital revolution. Electronics, it turns out, are eminently suitable for miniaturization. As the electronic components have gotten smaller, more of them fit in the same area. At the same time, the silicon wafers used in fabrication have become larger. The end result is the steady increase in performance and reduction in cost of electronics that we have come to expect. The transistors in a modern personal computer can be counted in the low billions (at the time of writing), and if they had to be fabricated serially a computer would be an astronomically expensive piece of equipment. Instead, batch processing gives us the relatively cheap piece of consumer electronics we are used to.

Plasma processing

Plasma processes, such as sputtering, reactive ion etching and surface modification were essential tools in all the work presented in this thesis, so here I will briefly explain what plasma is and why it is so useful in microfabrication.

Plasma may sound exotic and it is true that they are found in some very specialized applications, such as propulsion for space probes and growth of carbon nanotubes, but plasmas are also found in such everyday things as fluorescent- and neon lights, lightning and plasma torches for metal cutting. Perhaps the most obvious instance of a plasma in our everyday lives is the sun. This means that nearly the entire mass (99.9%) of the solar system is in a plasma state. So, plasmas are everywhere, and they are apparently useful, but what do we really mean by a plasma? Let's start with Irving Langmuir's original use of the word [21]:

"Except near the electrodes, where there are sheaths containing very few electrons, the ionized gas contains ions and electrons in about equal numbers so that the resultant space charge is very small. We shall use the name plasma to describe this region containing balanced charges of ions and electrons."
Irving Langmuir, 1928

While it is unclear why Langmuir chose to call it plasma, it is very clear what is meant. A plasma is an ionized gas (at least we will limit ourselves to the gas case): electrons have been separated from some of the atoms and molecules of the gas, leaving those particles as charged ions. The positive charges (ions) and negative charges (electrons) are distributed so that as a whole the plasma is nearly neutral. It should be noted that usually only a very small portion of the particles in the plasma are ionized, most are still neutral.

Plasmas can be divided in various ways depending on pressure, temperature and the degree of ionization. Temperature can be a tricky concept in a plasma. Because the electrons are so much lighter than the ions and neutral particles, they are often not in thermal equilibrium with the heavier particles and so have a different 'temperature'. The electron temperature is usually very high, several thousand degrees, while the ions in the same volume can remain at a much lower temperature, room temperature or up to a few hundred degrees. This is the case in all so called "cold" or "non-thermal" plasmas, which include all of the process plasmas used in the work presented here. Thermal plasmas on the other hand, where the ions are at the same high temperature as the electrons, are used for example in nuclear fusion.

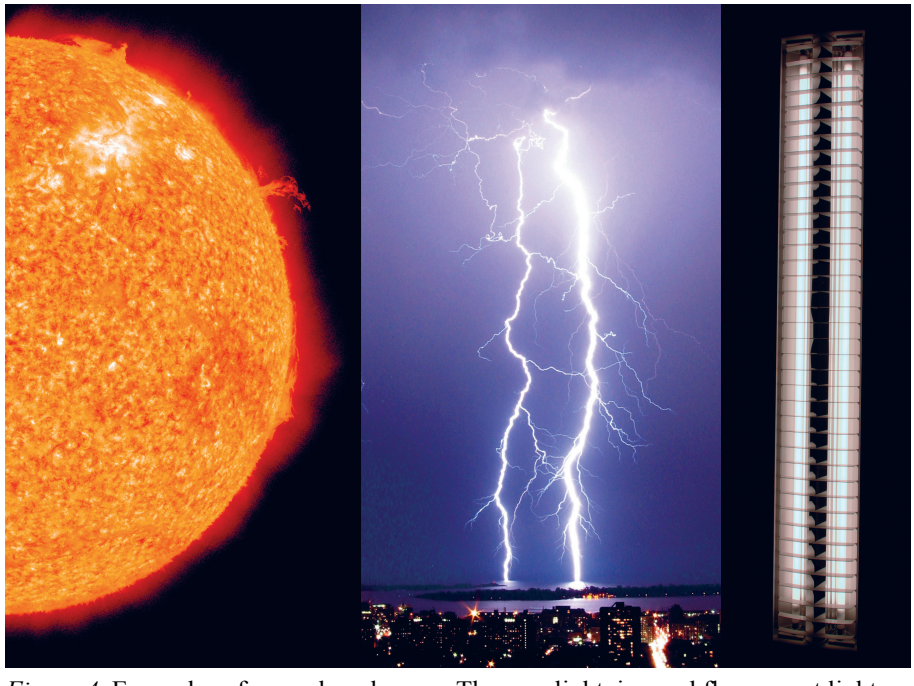

Figure 4. Examples of everyday plasmas. The sun, lightning and fluorescent lights; plasmas can be found at all temperatures and pressures. *Pictures of the sun and lightning by NASA and J.R. Southern respectively.*

Plasma processes

Various different properties of plasmas are useful in different applications. In the case of lighting, it is simply the emitted radiation one is after. In plasma processing for microfabrication, the plasma is primarily used as a source of charged and highly reactive particles. The process plasmas are typically low pressure plasmas (a few millibar up to a few tens of millibar), so vacuum systems are needed. As important as keeping a low pressure is keeping

good control of the gas mixture in the plasma and the vacuum system helps with this as well.

Below follow brief explanations of the techniques used in the studies presented in this thesis.

Sputtering

In sputtering, a form of physical vapor deposition, ions from a plasma (usually argon) are made to collide with a target material at high speed to 'knock loose' particles from the target. The sputter yield, the amount of material knocked out of the target per impacting ion, typically depends on material, temperature, impact energy, and impact angle. Particles or clusters of particles ejected from the target eventually settle on the substrate (or elsewhere in the vacuum chamber). Because the pressure during sputtering is relatively high, the particles of target material usually don't go straight from the target to the substrate but can bounce around a bit in the gas first. This leads to a more even coating of structured surfaces (*Figure 5*).

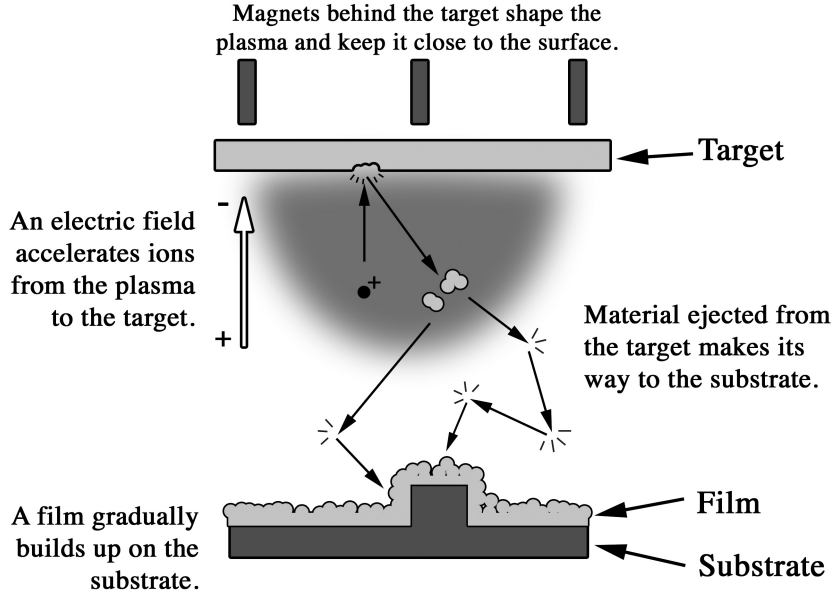

Figure 5. Schematic image of the sputter process. Material atoms or clusters are ejected from the target by ions accelerated from the plasma and make their way to the substrate. Collisions along the way means they arrive from different angles, allowing them to cover all sides of small structures.

There are many varieties of sputtering: one can use several different targets to produce alloys or layered structures or let a reactive gas into the chamber to produce for example oxides or nitrides.

Plasma Etching (dry etching)

When etching in plasma both the strongly reactive species in the plasma and the possibility of accelerating the ions in an electric field can be used to etch in ways that are not possible with any other system. For example, etching can be tuned to be isotropic, anisotropic or somewhere in between.

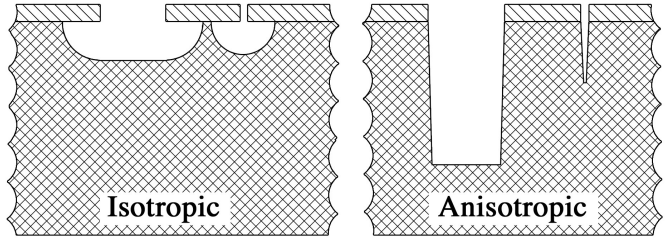

Figure 6. Examples of etch profiles in plasma etching. In isotropic etching, the material is etched at the same rate in all directions. Anisotropic etching means etching in some directions is faster. Ion bombardment leads to faster vertical etching.

When the etching is driven primarily by chemical reactions, it tends to be more isotropic and when it is driven by ion bombardment it tends towards anisotropic. There are also various ways to prevent the sidewalls being etched, to achieve more anisotropic etching. For example, adding oxygen when etching silicon in a fluorine containing plasma can create an oxide film on the sides. In the bottom of the pits, even a fairly gentle ion bombardment can prevent the formation of an oxide film so that etching there can continue. In the so-called Bosch process, isotropic etching of silicon is alternated with depositing a polymer film to protect the sidewalls. This way, even narrow structures can be etched very deep.

As with sputtering, plasma etching comes in many varieties depending on how the plasma is generated and how the ions and reactive neutrals are delivered to the substrate to be etched. Radiofrequency (RF) electromagnetic fields are often used to generate dense and stable plasmas. The frequency is typically 13.56 MHz, which is in the center of a frequency band set aside globally for industrial, scientific and medical uses. For the work in this thesis, an inductively coupled plasma (ICP) reactor was used. In such a system, energy is transferred to the plasma through electromagnetic induction. A coil outside the vacuum chamber acts as transmitter and the plasma acts as receiver, accelerating the electrons. An advantage of this kind of plasma generation is that there are no electrodes pulling charged particles out, so a very high plasma density is possible. To accelerate ions towards the substrate

being etched, an RF potential is applied to electrodes at the top and bottom of the reactor. This way the plasma also has a capacitively coupled part, which can be controlled separately and determines the potential difference (bias) between the substrate and plasma. The two RF fields have to be tuned together to deliver as much energy as possible into the plasma.

Figure 7. The ICP etcher. On the left, a schematic view of the etch reactor cut in half showing coil and electrodes for the two ways energy is coupled into the plasma. On the right, an ICP etcher with two chambers.

Some parameters to be controlled in ICP etching are gas mixture and gas flow, plasma density (controlled through the ICP power), substrate bias (controlled through capacitive power), pressure and substrate temperature. The gas mixture determines which reactive species are possible to achieve in the plasma. The gas flow will also determine which species are present by carrying reaction products out of the plasma chamber. The plasma density is important for how much of the ions and reactive species are present and so has a large influence on etch rate. The bias pulls ions toward the surface and together with the pressure determines how energetic the ion-substrate impacts are. Stronger ion bombardment can typically give a faster and more anisotropic etching, but can also lead to various problems with redeposited material and trenching (more on this in the chapter about diamond etching). Pressure, like plasma density, also affects how much of the reactive species and ions are present. The substrate temperature affects etch rate. In many cases, the substrate can grow very hot and has to be cooled.

All these parameters to play with give plasma etching great versatility, but also great complexity. Optimizing an etch recipe for a particular purpose is time consuming and the optimal parameters may vary between machines.

Surface cleaning and modification

Plasmas are also effective for cleaning surfaces from organic films and changing their surface chemistry. Since one does not want to damage the surface, the ion bombardment is kept to a minimum. Oxygen or air plasmas

are often used for cleaning surfaces and improving adhesion for sputtered metals and some photoresists. A long range of other chemistries can be used for surface modification.

Other important tools and methods

Other than plasma processing, there are a number of tools and methods necessary to produce microstructures. Here we will just very briefly mention some of the important ones in the scope of this thesis.

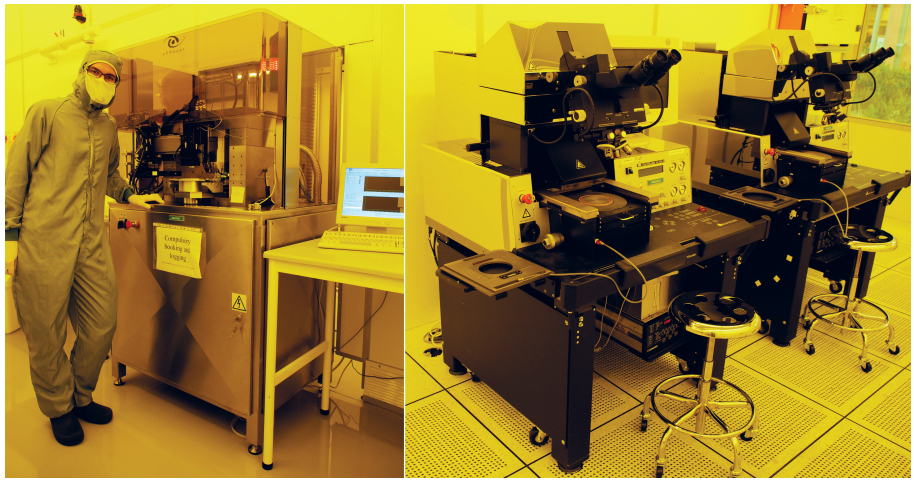

Figure 8. Lithography equipment. On the left a nanoimprinter and on the right two mask aligners for UV-lithography. Also on the left, an example of a cleanroom overall. Yellow light is used, as it does not affect the light sensitive photoresists. The floor in the right picture is perforated with many holes to control the airflow in the room.

UV- and nanoimprint-lithography

These two methods are used to copy a pattern from a master into a polymer film on a substrate. In UV-lithography, the master is a shadow mask, often chromium on glass, and the polymer film used is a photoresist sensitive to UV light. The mask is placed over the substrate and UV light is shone through it. The substrate is then developed in chemicals that dissolve either the polymer that was exposed to light (in the case of a so called positive photoresist), or that which was not exposed (negative photoresist). It is important that the gap between the mask and substrate is as small as possible during exposure to get good resolution. Even then, the method is limited by the wavelength of light used. Care also has to be taken to filter the light in the room from wavelengths that may affect the photoresist. This leaves a yellow or red light.

Nanoimprint-lithography is similar to embossing. The master has a pattern of raised areas that are pressed into the polymer film. The film can be a thermopolymer that is heated before the master is pressed into it and then cooled before the pressure is released. It is also possible to use a UV-curing polymer. It is very important that the pressure applied is even across the substrate, so air pressure onto a flexible film is used. The pressure is often several tens of atmospheres. Nanoimprint-lithography works down to very fine sizes, but is limited by proximity effects when patterns with very different scales are imprinted at the same time. After nanoimprinting there is also always a thin film of polymer left, even in open areas. This can be removed by a short plasma treatment.

Microscopy

One of the difficulties in microfabrication is that the structures are often too small to be seen with the naked eye. Various forms of microscopy are necessary, often after every process step, to see what is happening. The most common is optical microscopy. A good optical microscope can resolve features that are just a few tenths of a micrometer wide. Optical microscopes are fast and easy to work with, but for high magnifications they work with the sample very close to the lens and the focal depth is very shallow. This means that one can not tilt the sample much in high resolution optical microscopy and it can be difficult to get a good idea of the three dimensional structure of a surface. Special techniques, such as interferometry or confocal microscopy, can get around this to reconstruct 3D images, but at the cost of speed and simplicity.

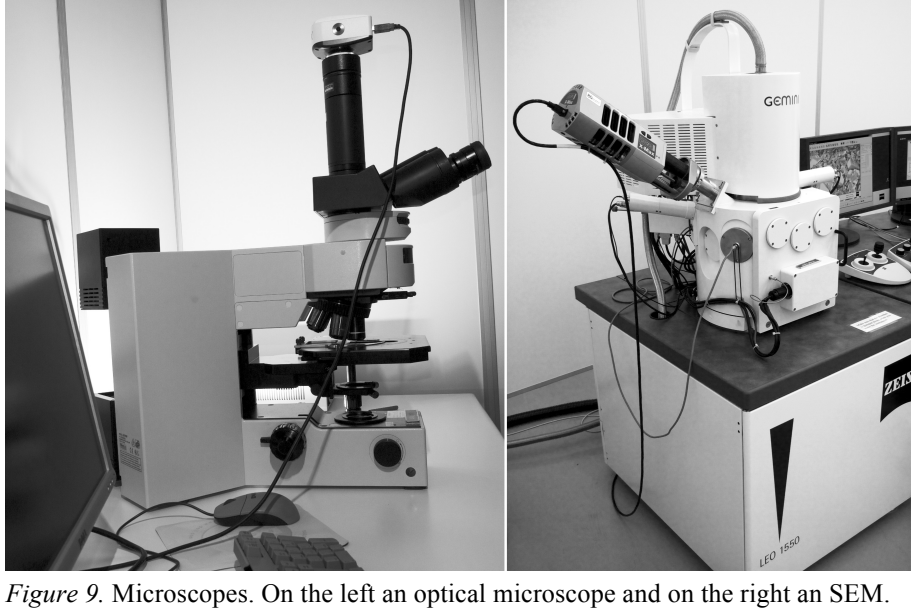

Figure 9. Microscopes. On the left an optical microscope and on the right an SEM.

In scanning electron microscopy (SEM), an electron beam is scanned across the surface and the amount of electrons coming back is detected. SEM can reach much higher resolution than optical microscopy, since it is not limited by the wavelength of light, and typically has longer working distance and focal depth. This means that one can tilt and rotate the sample to get a good feel for the shape of a surface (*Figure 10*). A drawback of SEM is that the sample has to be in a vacuum. This limits what kinds of samples can be looked at and it takes time to pump the air out after putting the sample in. It can also be difficult to produce good images of electrical insulators by SEM, as charges build up during scanning and distort the image.

For very fine structures on flat surfaces, atomic force microscopy (AFM) can give extremely high resolution and also quantitative measurements of height variations. It works by scanning a very fine tip, mounted on a cantilever, across the surface, either in contact with the surface, close above it, or some variation such as tapping the surface. Forces on the tip from the surface are measured by the deflection or changes in the vibration of the cantilever.

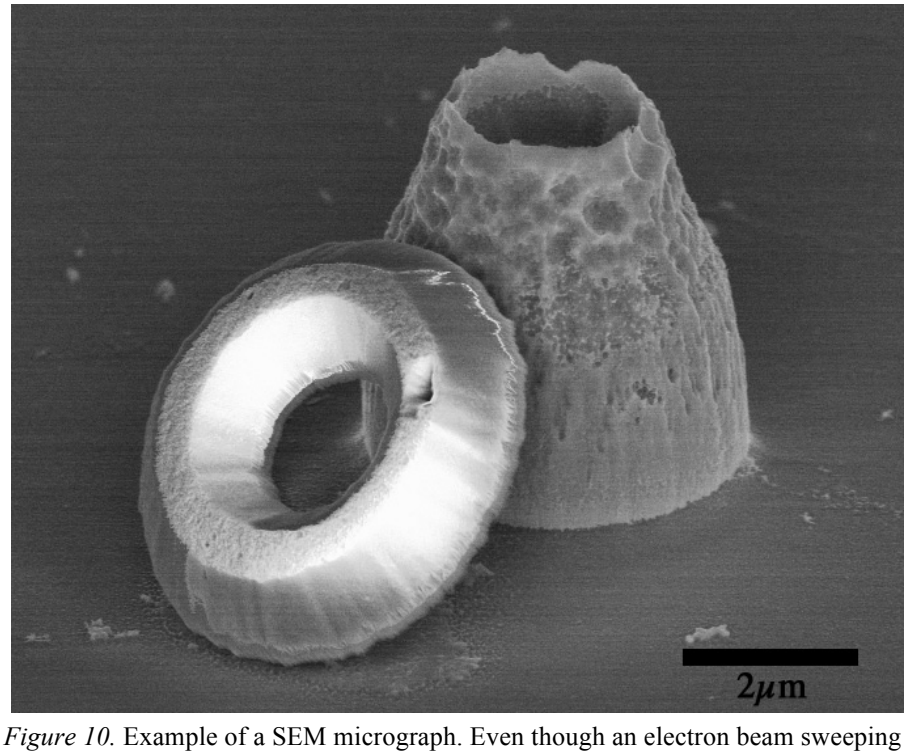

Figure 10. Example of a SEM micrograph. Even though an electron beam sweeping across the sample line by line generates the image and the contrast is due to different processes, interpreting an SEM micrograph can be nearly as intuitive as a photograph. Here we see a ring of nanocrystalline diamond leaning against a stump of silicon on a silicon surface.

Cleanroom

When working with very fine structures, even a single speck of dust in the wrong place can ruin a sample. To avoid this, the processing is carried out in a cleanroom, where the air is filtered and airflow carefully controlled to reduce the amount of particles. Special clothes are worn (*Figure 8*, left) to avoid spreading particles around and everything being brought in should be carefully wiped.

Materials

While diamond is a very interesting material, there are others that come in handy from time to time. Here are brief presentations of some that are of particular interest for this thesis.

Silicon

Silicon is the material used in nearly all microelectronics. Because of this, it is a very well studied material with a long list of standard processing methods, which have been adapted for other microsystems. High quality single crystal silicon wafers are available commercially at very reasonable prices. Silicon is a semiconductor but it is relatively easy to oxidise the surface to silicon dioxide, a good insulator. Diamond can be grown on silicon and it's a common carrier material for diamond films.

Aluminium

Aluminium is easy to sputter, can be etched by both wet and dry etching and is relatively easy to remove. This has led to it being a very popular masking material.

Polydimethylsiloxane (PDMS)

PDMS is a very popular material for microfluidic prototyping [22]. It is a two-component silicone rubber that is suitable for replicating fine details by casting. After mixing the base and curing agent, PDMS can be cured at room temperature, although curing is much faster at higher temperature. The cured PDMS is relatively inert to many chemicals although it can swell in many solvents. PDMS can be bonded easily to itself, glass and several other materials after treating the surfaces with air- or oxygen plasma. Removing PDMS after bonding is difficult, but can be done with concentrated sulfuric acid.

Diamond etching

Diamond is hard, and chemically inert at room temperature. It follows that diamond is difficult to shape. Laser ablation is possible (though it can be difficult on a transparent surface) as is growing diamond by CVD on a structured substrate. Both of these come with limitations in terms of surface quality of the diamond and laser ablation is limited in resolution and speed. We have seen that in microfabrication etching is often the preferred method to shape a surface, either chemical etching (wet or dry) or physical etching by ion impacts. Wet etching of diamond is very difficult (it may be etched by some molten salts and metals at high temperature), but dry etching with oxygen and argon ion beams has been done for three decades [23] and in reactive plasmas for at least two and a half [24]. Dry etching of diamond is relevant to all of the papers in this thesis except **papers V and VII**. In particular **papers I and IV** deal with developing etch techniques. To etch the diamond surface at any appreciable rate in an oxygen plasma, high plasma density and ion energy is necessary, and it is still much slower than for example silicon etching. As the etching requires such strong ion bombardment it is anisotropic with walls sloping slightly outwards from the mask (*Figure 6*). Several mask materials have been used for diamond etching by various groups, the most common are aluminium [25-28] and silicon oxide [26, 29], but there are many variations, like polymer resists (to transfer continuous structures) [25], silicon nitride [26], spin-on glass [2, 30], gold [26], titanium [26], nickel [31] and metal naphtenates [32]. In this thesis, aluminium is used, since it gives good selectivity and is easy to deposit and remove. The purpose for the process development in **paper I** was producing the achromatic half wave plates and annular groove phase masks described in **papers II and III** and the next section. The angled sidewall etching in **paper IV** was developed with a waveguide ATR concept in mind, which will be described later.

Patterning

The first problem encountered when working with microfabrication on diamond substrates has to do with them typically being quite small. The pure diamond samples we have worked with have all been smaller than 2 cm in diameter and often much smaller while most of the equipment and techniques used for processing them have been developed for wafers larger than five centimeters. Particularly in patterning this led to difficulties. When one

has such a small sample to work with, the whole surface becomes precious. On a larger wafer, losing a few millimeters around the edge to the edge bead from spin coating is rarely a problem, but on a small sample those millimeters may constitute most or all of the substrate area. Edge bead is a thickening of the polymer at the edge that forms during spin coating, similar to a how drop of water hangs at the end of a blade of grass. The width and thickness of the edge bead depend on the thickness of the polymer film being spun out; a thin film is spun at a faster speed and forms less edge bead. The part of the sample that is under the edge bead is usually lost, buried under a much thicker polymer layer than the rest of the substrate. In UV-lithography, edge bead also leads to problems in getting the mask close enough to the substrate for good resolution (This is what happened to the diamond ring in *Figure 10*, the hole in the middle was not present on the mask but appeared due to bad mask contact in the UV-lithography).

Figure 11. Edge bead. Edge bead forms around the edges of a substrate during spin coating. In UV-lithography it can lead to a gap between mask and substrate.

On larger wafers, the mask and wafer can flex a little, so that the contact is good away from the edge. For larger structures, such as those in **papers VI** and the waveguides in **paper IV**, resolution may be good enough even on small samples. The micrometer and sub-micrometer features of the gratings in **papers I-IV**, however, would be difficult even with good mask contact. Electron-beam (E-beam) lithography is certainly capable of those feature sizes, but it is a slow and expensive method, particularly since we did not have access to it on site, and we needed to do a lot of etch tests. Instead we turned to nanoimprint-lithography for transferring those fine structures to our diamond substrates. That way we could replicate the pattern from a single master, written by E-beam or laser, many times. At first we used nickel stamps, replicated from the original wafer by electroplating, for the nanoimprinting. Nickel is stiff and even with a thin stamp we had a similar problem as in UV-lithography; several millimeters inside the edge bead were not patterned even when using a very thin polymer film. Cutting the nickel stamp so that it was smaller than the inner radius of the edge bead helped, but some problems related to the stiff stamp remained. One was that particles on the surface could hold the stamp up and cause large blank areas in the pattern. Another problem was due to the polycrystalline substrate having small height variations between crystal grains, typically a few tens of nanometers. This led to the imprint depth and residual polymer thickness being different between grains.

To get around these problems we switched to a soft PDMS silicone stamp, which was cast directly on the master wafer written by laser or E-beam. The PDMS molding did not damage the original so many copies could be made, in contrast to the nickel-plating, which destroyed the master wafer. The nanoimprint parameters had to be changed to suit the softer stamp: a lower pressure, higher temperature and longer imprint time eventually gave good results. The soft stamp could bend around particles, edge bead and steps at grain boundaries to give a homogeneous pattern across the substrate. Care had to be taken when placing the stamp on the substrate however. If the stamp was bent or stretched during placement, it did not always relax afterwards, which resulted in distortions in the pattern. Edge bead could still not be completely eliminated, but by using a thin enough polymer film, it could be kept to around half a millimeter from the edge. The soft stamp turned out not to give very good results in thick polymer films, so a thin film (~200 nm) was preferable in any case. It should be noted that a PDMS stamp is only suitable for transferring dense patterns of small and shallow features. If the features are of a scale on which the stamp can deform significantly (~10 µm in this case), it will bend around them. Having a range of suitable stamp materials on hand, so that one could match the stiffness of the stamp to the pattern being imprinted would be ideal. In our case however, the PDMS stamp worked very well.

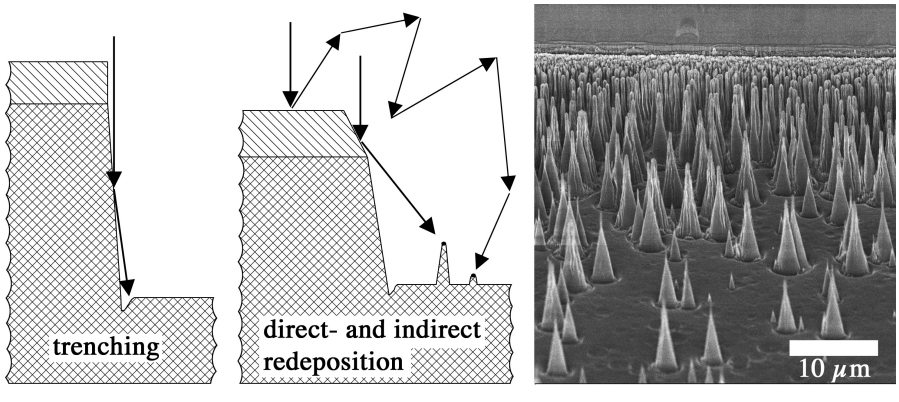

Figure 12. Typical problems in diamond etching. Trenching caused by glancing incidence of ions on the sidewalls and redeposition of mask material either directly or indirectly. On the right can be seen an example of the structures that may form due to redeposited material. Spikes have formed from micromasking by redeposited aluminium. Densely packed close to the wall (at the back) and sparser further away from it. Note that there is trenching around the bottom of the spikes.

Etching

Many problems common to etching with heavy ion bombardment can be seen in diamond etching, such as trenching, mask erosion and faceting, and redeposition of mask material (*Figure 12*). Trenching is the formation of trenches at the bottom of sidewalls. It is caused by ions redirected by glancing hits to the walls. The mask erosion is due to physical sputtering by energetic ions. The sputter yield is often angle dependent, giving rise to faceted edges. Material sputtered from the mask may be deposited on the surface being etched, either directly or by backscattering from the gas, and give rise to micromasking. In **paper I** we describe how mask erosion at the edges of an aluminium mask was particularly problematic when etching a deep grating of fine lines, where no part of the mask is far from an edge. In order to etch these gratings with well defined square tops, the mask had to be made more than five times as thick as that needed to protect a flat surface away from the edge.

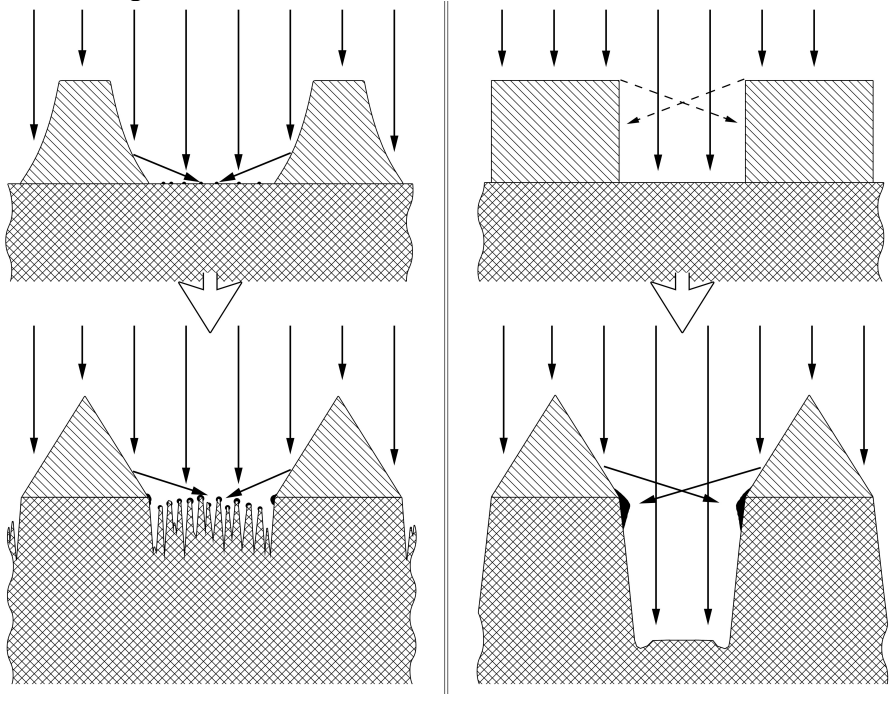

Figure 13. The importance of initial mask profile. From an angled sidewall (left), direct redeposition at the onset of diamond etching causes micromasking which leads to microvilli. These in turn are masked further as the etching goes on. If the mask initially has straight sides (right), very little direct redeposition occurs at the onset and what little there is may stick to the mask on the opposite side if the mask is thick enough. Later in the etching when sputtering and redeposition from the faceted mask is more severe, the groove is deep enough that all of it sticks to the opposite side. Figure adapted from **paper I**.

With such a thick mask and rapid sputtering from many edges, a lot of material was being removed and redeposited elsewhere. In the case of redeposition however, etching gratings turns out to be advantageous. Rapid sputtering of the mask takes place at angled edges, and the material sputtered from the edges has a narrow angular distribution. If the mask was made with vertical sides at the start, only very little direct redeposition took place in early etching. Once the mask had developed some faceting and more material was being redeposited, the grooves were already deep enough that most sputtered mask material was caught on the opposing wall (*Figure 13*). This probably helped preserve the mask to some extent, but also made the grooves a bit narrower with depth and the walls a bit striated. The most important thing however was that it kept mask material off the bottom of the grooves, so that the etched surface was smooth and the etch rate predictable.

Another way to avoid problems with redeposited mask material that has been used by many groups is to add a bit of fluorine to the etch plasma [26-29], usually in the form of SF_6 or CF_4. This also increases the etch rate of the mask, so it was not an option when etching the deep gratings of **papers I-III**. In **paper IV** however, we used this faster mask etching to control the sidewall angle of etched structures. The sidewalls usually had two distinct slopes with a steeper lower part and a shallower upper part. These were produced before and after the full faceting of the mask respectively as described in *Figure 14*. The upper slope could be controlled by varying the proportion of SF_6 in the etch plasma while the lower slope depended mainly on the bias power (although only small variations were possible). Because the method depended on a continuous removal of the mask, a thick mask layer was again needed, just as for the deep gratings.

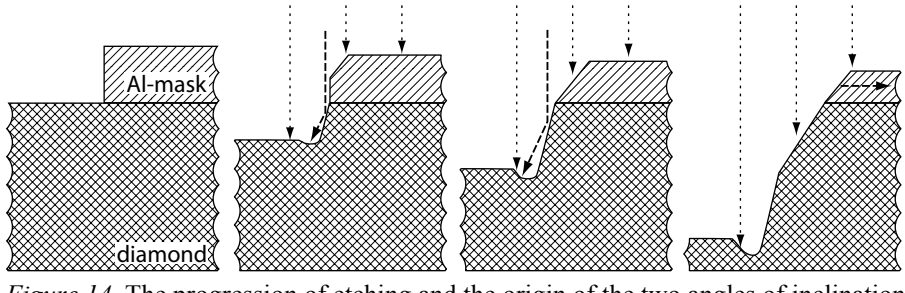

Figure 14. The progression of etching and the origin of the two angles of inclination of the sidewall. (from left) The initial mask profile is vertical. In early etching, before the mask is fully faceted, the edge of the mask does not move. The sidewall etched in diamond is slightly inclined because some ions are deflected instead of etching the wall. Once the mask is fully faceted the edge starts receding. The angle etched in diamond then depends on the etch rate ratio between the mask material and diamond. Figure adapted from **paper IV**.

As the mask receded, its edge was smoothed out. This resulted in the upper slope being much smoother than the lower, which often showed a lot of striations carried over from a rough mask edge. Starting the etching with a mask already faceted by argon sputtering could produce structures with nearly none of the lower slope. In the case of free-hanging waveguides, the lower slope could be etched away by continuing etching after the diamond film had been etched through.

Masking

The thin polymer mask from the nanoimprinting did not last long enough in a chlorine plasma to etch the thick aluminium layer required as mask during diamond etching. And as noted above, increasing the polymer thickness led to wider edge bead and lowered pattern fidelity in the pattern transfer. Instead, a layered approach to masking was adopted. Three masking layers were sputtered onto the diamond substrate prior to spin coating and nanoimprinting: First the thick aluminium layer and on top of this a thin layer of silicon and then another, thinner, aluminium layer. The nanoimprinted polymer was then used as mask only for etching the thin aluminium layer, which was used as mask to etch the silicon, which was used as mask when etching the thick aluminium layer. This added a few steps to the masking process, but allowed for a thick aluminium mask to be produced without losing the advantages of a thin polymer film in the nanoimprinting. Since the masks could be made more than thick enough for each etch step, the etching could be extended so that more small spots and defects could be removed. Also, the line width could be fine tuned somewhat by varying the length of the silicon etching.

To get vertical sidewalls in the aluminium mask, an etch recipe with periodic etching and oxidation of the surface was developed. Aluminium was etched in chlorine containing plasma; the surface was then exposed to oxygen plasma so that a thin film of oxide was formed. In the next cycle, the oxide film at the bottom was quickly removed by ion bombardment during aluminium etching, while the walls were protected from etching. This etch process, which was inspired by the Bosch process for etching silicon, produced a wavy but essentially vertical wall. Nanoimprint polymer, unlike silicon, is etched rapidly by oxygen plasma, so the layered masking approach not only allowed for a thick mask to be produced but also turned out to be necessary for this method of etching vertical sidewalls in aluminium.

With all these process steps in place it was possible to fabricate the deep, steep sided gratings for half wave plates and annular groove phase masks (**papers II and III**), tall pyramidal structures for broadband antireflective surfaces and smooth, inclined facets at the ends of a waveguide (**paper IV**). For the superhydrophobic surfaces (**paper VI**) and microelectrodes (**paper VIII**), conventional UV-lithography and masking were used.

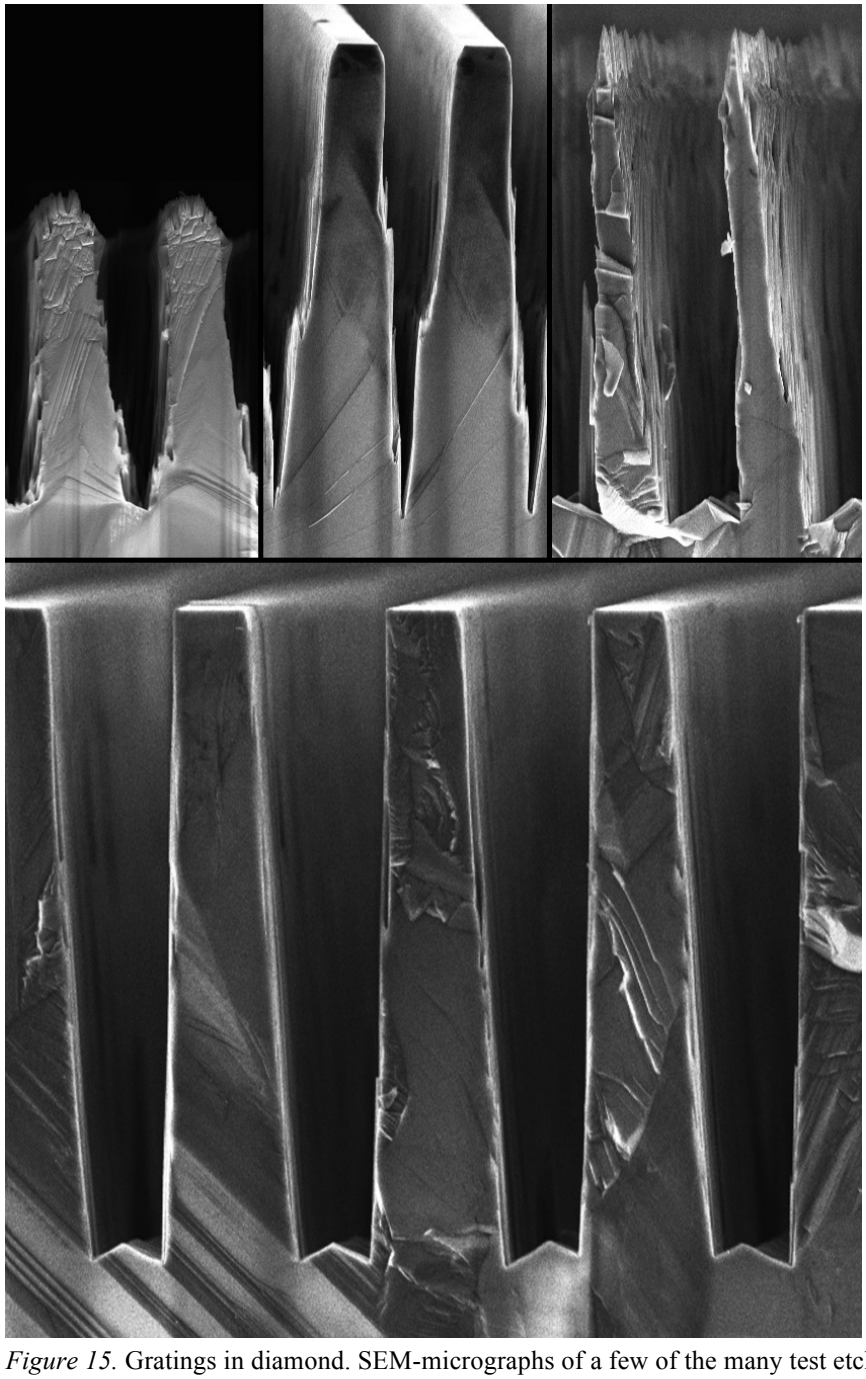

Figure 15. Gratings in diamond. SEM-micrographs of a few of the many test etchings required to come up with a working process (upper row) and a grating etched with the final masking and etching process (bottom).

Sub-wavelength gratings in diamond: Antireflective gratings and annular groove phase masks

Light behaves quite different when it hits something smaller than its wavelength compared to when hitting a larger object. For example, sunlight scattering on molecules in the atmosphere gives the sky its blue color, while scattering on drops of water makes clouds look white. In the case of gratings, when the period falls below the wavelength (in both the incident and transmitting medium) of the light shining on it, we leave the realm of diffraction gratings behind. Instead, light behaves as if the grating is a film of a continuous medium with properties determined by the morphology of the grating and the optical properties of the materials in it. So by designing the shape of the grating, one can design the optical properties such as refractive index and how it alters polarization states.

Antireflective gratings

As light crosses an interface between two media with different refractive indices, some of the light is reflected. The higher the difference in refractive index, the more is reflected. It is often desirable to avoid this reflection. On glasses, because reflections can distract or even blind the wearer; and in lenses for cameras and other optical instruments, to get as much light as possible through and avoid flares and errors caused by reflected light.

The simplest way to reduce the reflection is to introduce a film with an intermediate refractive index at the interface. The reflections from the top and the bottom of the film can then be made to interfere destructively, cancelling both (*Figure 16*). For perfect cancellation, two criteria must be fulfilled: the intensity of both reflected beams must be identical and they must be 180° out of phase. The first criterion means the refractive index of the film (n_f) must be just right with respect to those of the incident medium (n_i, usually air) and the substrate (n_s). The second criterion puts a constraint on the film thickness (d) and the incidence angle (θ_i) with respect to the wavelength (λ). In the case of normal incidence ($\theta_i = 0$), the film should be an odd number of quarter wavelengths thick ($d = m \lambda / 4 n_f$, where m is an odd integer). So even if

one can find a material with just the right refractive index and deposit it with just the right thickness, the reflection will only be perfectly suppressed for specific wavelengths and incidence angles.

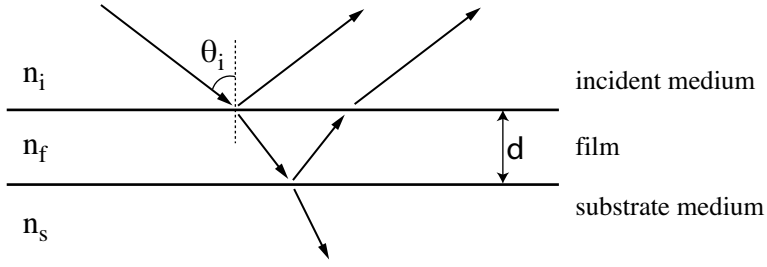

Figure 16. Reflections in a film on a substrate. (Figure adapted from [33])

Even when a material with a suitable refractive index exists for an antireflective coating on a particular substrate, it might be unsuitable for other reasons. For example, there may be adhesion problems, or the material might be toxic or water-soluble. For diamond some of the desirable surface characteristics, such as the physical robustness and chemical resistance, would be lost if one were to add a film of a different material.

As mentioned above, when light interacts with a grating with a period shorter than the wavelength of the light, the grating behaves as a film of continuous material. The refractive index of this equivalent film will be somewhere in between those of the materials making up the grating and can be chosen freely in this range by designing the grating right. The more of the substrate material that is present in the grating, the closer the optical properties will be to that of the substrate and vice versa. The exact relationship between fill factor (the fraction of substrate material present in the grating) and refractive index is not so simple, but the refractive index can be calculated for any given grating. In general, the grating does not even need to be the same in all directions, so the refractive index can be different along different directions or polarization of the light. For example a one-dimensional grating (*Figure 17*) will be birefringent. A regular two-dimensional grating on the other hand, is much more isotropic and gives rise to less birefringence. For the work presented here, all calculations have been made using rigorous coupled wave analysis (RCWA), in which the structured is divided into layers and Maxwell's equations are solved from layer to layer.

A binary grating (a grating with only two levels) can be used to cancel reflections instead of a film of a different material. This way one can avoid adhesion problems and since the effective refractive index can be chosen by design, it can be chosen to give the lowest possible reflectivity. The grating will still be optimized only for specific wavelengths (*Figure 18*) and incident angles, but in many applications only a narrow wavelength band and a narrow angular distribution of incoming beams are of interest.

A downside of these gratings is that they require very high precision in the fabrication. Small deviations in any of the grating parameters can reduce the effectiveness. High precision in grating period is easy, the width of grating asperities can be more challenging to control and achieving the correct depth, especially in deep gratings, can be quite difficult. When making the binary antireflective gratings in **papers I-III**, the influence of the somewhat sloped sidewalls and trenching at the bottom was hard to estimate, so optical transmission measurements were used to optimize the etch time.
Antireflective coatings can be made to work over wider wavelength bands by stacking two or more films on top of each other. An equivalent grating structure would have two or more steps, each level being equivalent to a film. Taking it one step further, a gradient refractive index can be produced by a grating with continuously sloping sides. If the fill factor varies from 0 at the top of the grating to 1 at the bottom, the resulting refractive index gradient varies continuously from that of the incident medium to the substrate medium. Such gradients can be very effective in reducing reflections, both over broad wavelength bands and for a wide range of incident angles. Ideally such structures should be quite deep, but even at shallower depths big improvements over binary gratings can be had (*Figure 18*). Even when the target application only requires a narrow wavelength band and normal incidence, continuous structures have the advantage of not being as sensitive to the depth of the grating.

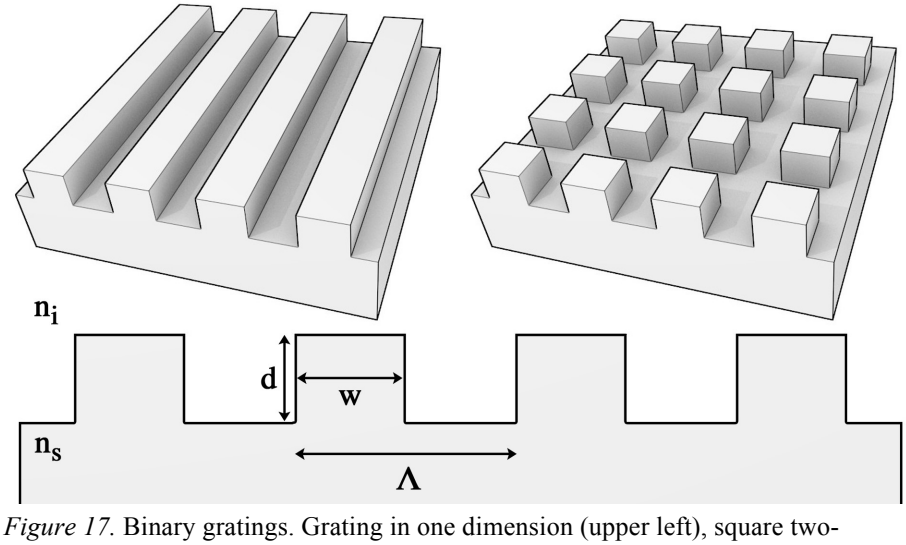

Figure 17. Binary gratings. Grating in one dimension (upper left), square two-dimensional grating (upper right), and definitions of some parameters (bottom): refractive indices of the incident and substrate material (n_i and n_s), depth and width of asperities (d and w), grating period (Λ).

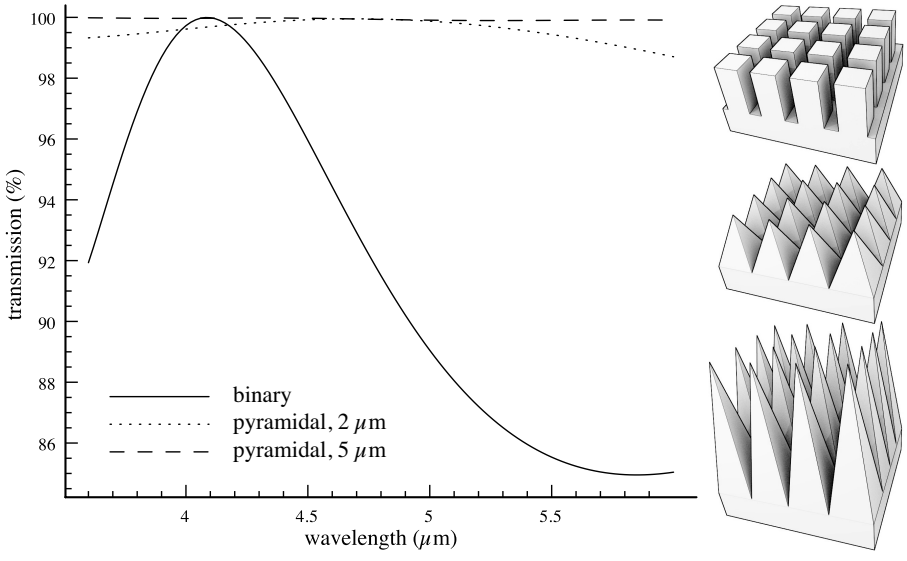

Figure 18. Transmission across an interface between air and diamond structured with binary and pyramidal gratings. The binary grating with Λ=1.5 μm, w=0.975 μm and d=2 μm and the pyramidal with Λ=1.5 and depth 2 or 5 μm. The transmission of the deep pyramidal grating varies between 99.90% and 99.98%. RCWA calculation.

In **paper IV** we demonstrated such a broadband antireflective structure in diamond by etching angled sidewalls, as described in the previous section. The grating profile used in **paper IV** is a kind of broken pyramid shape**,** with a steeper lower slope and a more shallow upper slope. This shape was due to the etch process used, but turned out to have some advantages. Over the investigated wavelength regime (10-50 μm), the broken pyramids compare favorably to regular pyramids with the same depth. In the calculations, they give a slightly lower transmission at some shorter wavelengths, but a higher transmission at longer (*Figure 19*). Since the tips are not as narrow, they should also be somewhat more robust.

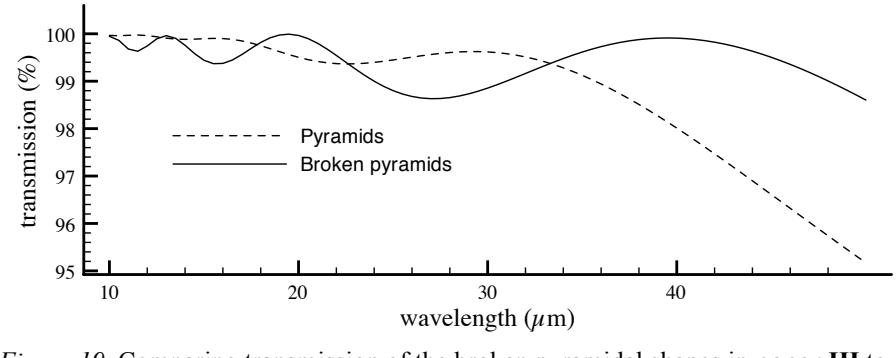

Figure 19. Comparing transmission of the broken pyramidal shapes in **paper III** to pyramids. The depth is 13.3 μm for both. RCWA calculation.

To reach the kind of near perfect transmission seen in *Figure 18* for these longer wavelengths, a much deeper pyramidal grating is needed. To achieve better than 99.7% transmission between 10 and 50 µm, a 40 µm deep pyramidal grating would be required, much deeper than would be practical to etch with the methods in **paper IV**.

The transmission measurements in **paper IV** were carried out on a diamond substrate etched on both sides to get as accurate measurements as possible. The etched structures had slightly wider tips and a small step where the lower and upper sections meet. The structures on the two sides were also slightly different. All this was taken into account in an attempt to calculate the transmission. The result and how it compares to the measured values can be seen in *Figure 20*, as can the actual structure and the simulated one (note that the values in this figure are for transmission through both sides while those in *Figure 18* and *Figure 19* are for just one side). While the measured spectrum doesn't agree perfectly with the calculated, the predicted peaks and valleys are clearly there. That the actual transmission is one or two percent lower than the calculated is likely due to imperfections in the structure.

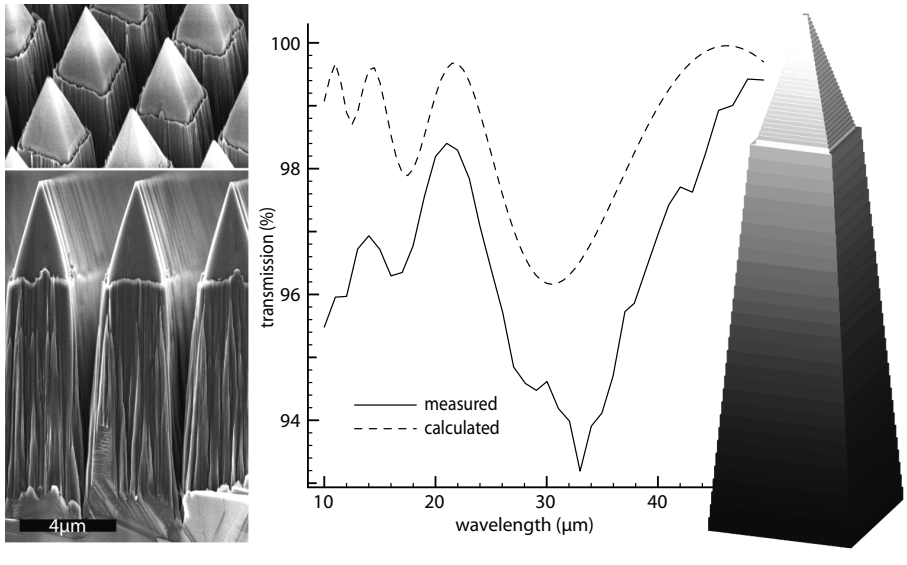

Figure 20. Fabricated broadband antireflective structures (left) and the structure used to simulate them (right). The measured and calculated transmission for a two sided sample can be seen in the middle. Figure from **paper IV**.

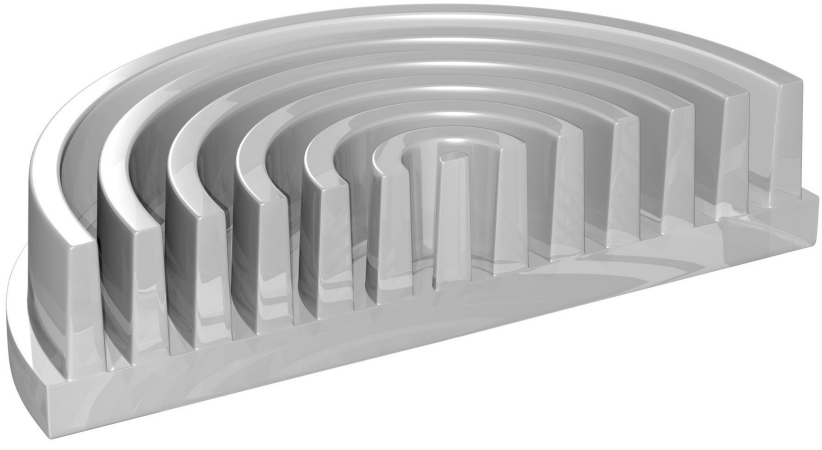

Figure 21. Illustration of the center of an annular groove phase mask cut in half.

Annular groove phase masks

Exoplanets

One of the most exciting scientific developments in recent years has been the discovery of exoplanets, or extrasolar planets, planets in orbit around stars other than our own sun (or floating free in interstellar space, though the definition of planet is then less clear). First, in the early to mid 1990s, there were a few, then a few more, and then lots and lots. At the time of writing, over 800 planets had been discovered orbiting around 650 stars (exact numbers vary according to what criteria for discovery are used). Several thousand possible detections of exoplanets are awaiting confirmation, so the list is set to be in the thousands soon. Most of these planets were discovered either by observing the way a star's colour changes slightly as a planet's gravitational pull make it "wobble" (radial velocity method) or by the very small change in the star's brightness as the planet passes in front of it (transit method). Both these methods have an easier time of finding large planets with short orbital periods. Finding all these planets has fuelled the interest in whether they might harbor extraterrestrial life, but the methods of detection only tells how far the planet is from its star and its mass or size. This can give some idea of the temperature and, in cases where both the size and mass are known, the density, of the planet. This certainly puts some bounds on the habitability of a planet, but more data is required to say whether a planet is actually likely to harbor life or not. A spectrum of light that has passed through the planets atmosphere (if it has one) would tell a lot about its chemical composition and give important clues about what might be found on the surface. The specifics of what might be detected depend on what wavelengths of light the spectrum covers. One way of acquiring such a spectrum

is to measure the change in the spectrum of the star as the planet passes in front of it and a tiny portion of the star's light passes through the planet's atmosphere. This is of course only possible for planets which transit directly in front of their parent stars as seen from our point of view. The probability of this happening for a planet orbiting a star as big as our sun at the same distance as that between the Earth and sun is around one half of a percent. This probability increases for planets closer to the star and decreases for those further away. Transits are also far in between and only last for a few hours. If, on the other hand, one can measure directly the light reflected or emitted by the planet, separately from that of the star, it is possible produce spectrums even for planets that do not transit in front of their stars. It also allows for the detection of planets with very long orbital periods, which might require many decades or centuries of observations to detect with the radial velocity or transit methods. The problem that has to be overcome to make a direct observation is to separate the faint light from a planet from the much brighter star when they are orbiting close together at a literally astronomical distance from the observer [34]. This has been done, but the method is most suited for large planets orbiting far from a star (*Figure 22*). To improve these images and to image smaller planets and planets with smaller orbits requires large telescopes with adaptive optics (at least for telescopes on the surface of the Earth), but also improved coronagraphs.

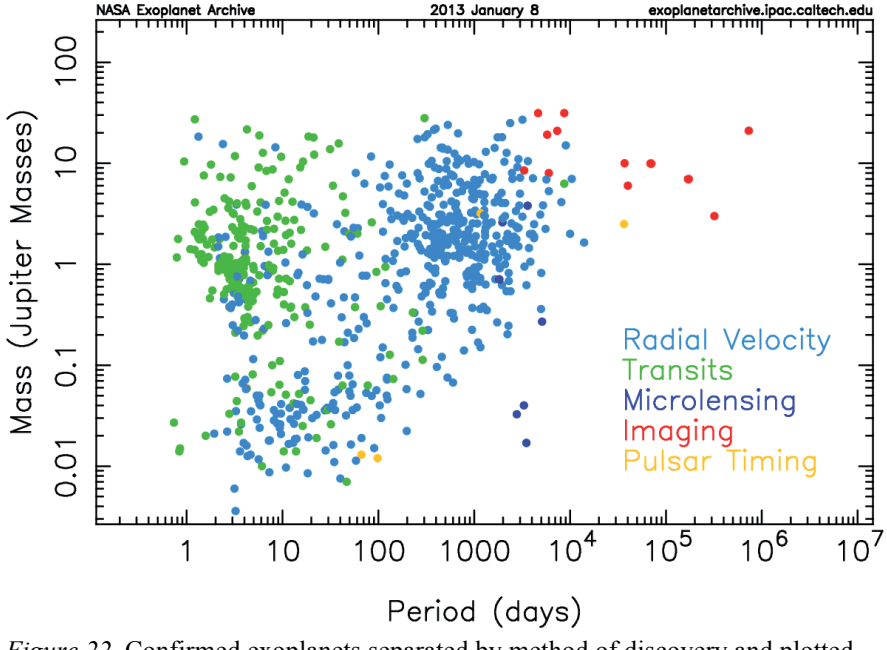

Figure 22. Confirmed exoplanets separated by method of discovery and plotted according to orbital period and mass. *From NASA Exoplanet Archive operated by the California Institute of Technology.*

Coronagraphs

A coronagraph is a part of a telescope that filters the light from a bright source in order to make faint nearby sources visible. As the name implies, this usually means blocking the light of the sun in order to see the corona (the sun's upper "atmosphere"). New instruments of this kind are however becoming sensitive enough to observe exoplanets directly, at least if they are relatively large and orbiting far from their star [35, 36]. To observe planets as close to a star as possible, or around stars further away, coronagraphs with a small inner working angle (the smallest angular separation at which a faint planet can be detected) are being developed. One group of such coronagraphs is optical vortex coronagraphs.

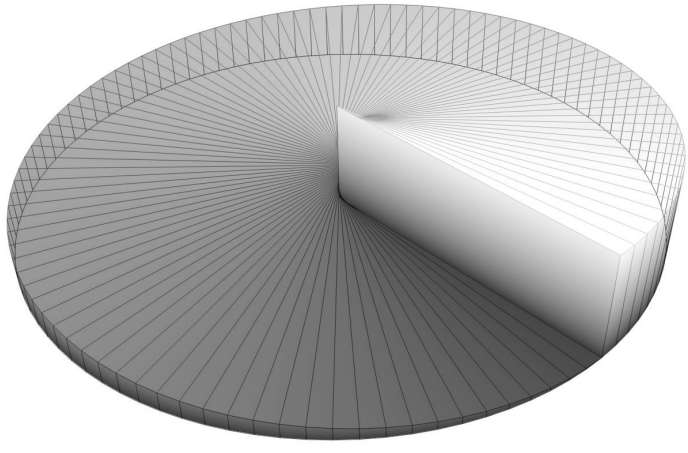

Figure 23. Illustration of a helical ramp phase mask for a scalar optical vortex. Fabricating such a component with good precision in thickness and a well-defined center would be difficult.

An optical vortex occurs when the phase of light is ramped continuously around the optical axis. The optical vortices discussed here will all change the phase a total of 4π as one goes all the way around the vortex. At the center of the vortex there is a so-called phase singularity that forces the amplitude to zero rather than allowing the light to have an infinite number of phases at once. Another way of seeing it is that as one approaches the center, any beam of light will find another with a phase shifted by π to cancel it out. What this cancelling out means in practice is that light going through the center of the optical vortex (which with a properly aligned coronagraph should be the light coming from the star, along the optical axis) is scattered outside the image and can be blocked by a diaphragm. The phase ramp needed for an optical vortex can be produced by varying the thickness of a transparent medium helically around a central axis (*Figure 23*). However, achieving sufficient precision in thickness and a well-defined center is no easy problem to solve. Further, the phase shift of such a ramp depends

strongly on the wavelength of the incoming light and will therefore not be optimal for use in astronomy, where fairly broad wavelength bands are often of interest.

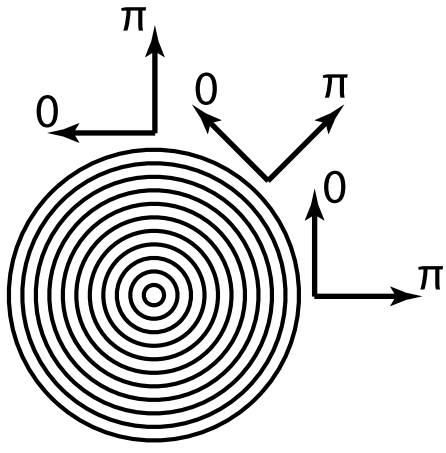

Figure 24. Illustration of the relative phase shift between two polarization components around an optical vector vortex. As one moves a quarter turn around the center, the difference in phase between parallel components is π. It is not difficult to convince oneself that destructive interference should occur close to the center.

An alternative to this simple scalar optical vortex is a vector vortex, which instead of simply varying the phase changes the direction of the polarization vector continuously around the central axis [37]. A vector vortex can be produced by a circularly symmetric half-wave plate. A half-wave plate is a birefringent device which shifts the phase between polarization components by π (a half wave). Various vector vortex coronagraph (VVC) concepts exist, differing in the way the circular half-wave plate is constructed. Possible routes include controlling the birefringence direction in liquid crystal polymers, using the birefringent properties of artificial photonic crystals and using the birefringence of sub-wavelength gratings. Birefringence in a one dimensional sub-wavelength grating, such as that seen in *Figure 17*, can be understood intuitively. It is reasonable that the component of the light parallel with the grooves 'experiences' a different material than that perpendicular to them. A circular sub-wavelength grating forming a circularly symmetric half-wave plate is called an Annular Groove Phase Mask (AGPM). Such AGPMs have several advantages. By controlling the shape of the grating the birefringence can be controlled in detail and in particular, it can be made to be nearly wavelength independent over wide wavelength bands (this is discussed in **paper II**) while other VVCs work in narrower bands. The AGPM also has the advantage of a well-defined center, something that is difficult to achieve with liquid crystal polymers. Finally, a grating can be made to work at longer wavelengths where materials with the right properties for other kinds of half-wave plates are not transparent. In fact, the grating becomes easier to manufacture at the larger scales needed for longer wavelengths. The

opposite is also true, which may be a drawback of the sub-wavelength gratings: they are difficult to produce for short wavelengths. So they can be seen as complementary to, rather than competing with, the other approaches since they are most suitable for different wavelengths.

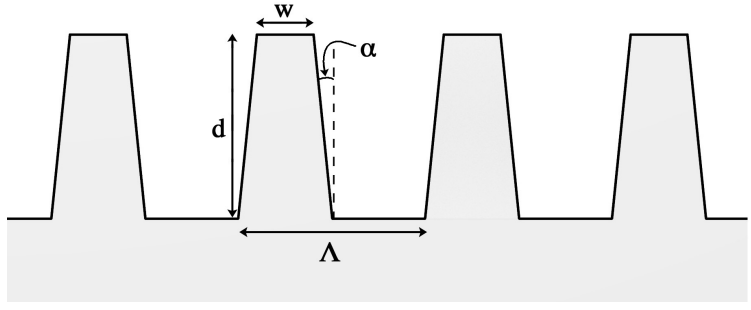

Figure 25. Grating parameters in a grating with a trapezoidal profile. Depth d, width w (defined as the width at the top of the wall), period Λ and sidewall angle α.

Fabricating AGPMs

An AGPM should be easier to produce than the kind of helical ramp needed for a scalar optical vortex. While the precision required in the grating parameters is certainly not easy to achieve, at least the grating is (ideally) binary. Optimal grating parameters were calculated by RCWA, taking into account expected fabrication limitations. These optimizations were then re-calculated as the fabrication process was developed and better estimates of sidewall angles and achievable aspect ratio became available. The fabrication procedure described in **paper I** was painstakingly developed to produce an AGPM for the upper half of the N-band, centered around 12 μm (**paper II**). Even after managing to produce gratings with the high aspect ratio we needed, the difficulty remained to produce a sample with both the correct wall width and the correct depth. The width was difficult to control with high enough accuracy but easy to measure. The depth on the other hand could in principle be precisely controlled by adjusting the etch time, but it was more difficult to measure. The grooves were too deep for AFM and too narrow and deep for white light interferometry (the triangular ridge along the bottom, seen in *Figure 15*, probably played a role in weakening the signal in the interferometry as well). Cracking the diamond sample and looking at the cross section in the SEM gave the best measurements of depth and sidewall angle, but destroyed the sample. The depth could also be measured by carefully measuring the distance between a point at the top of the grating and one at the bottom in several SEM micrographs taken with different tilt angles. This method was time consuming, but was found to give good precision. In order to reach a precise depth, it was desirable to measure the depth and then continue etching if necessary. These measurements were more difficult as they had to be made without removing the mask, and it was often hard to determine

exactly where the top of the diamond wall was. Even so, a precision in depth of around 100 nm could be reached. We did not have sufficient control of the nanoimprint- and mask etching processes to reach the precision required in line width (tens of nanometers). Instead, the width of the lines was measured after masking and an optimal depth for the given line width was calculated. This allowed for a much lower precision requirement in the width while compensating with the depth to produce a nearly optimal grating.

The etch process was precise enough that when we started working on the much finer gratings, meant for the L-band (3.5-4.1 μm) in **paper III**, even the first test had the well-defined trapezoidal cross section we were after. However, producing a grating with close to optimal parameters was still more difficult for the L-band. This was due to two reasons: first, measuring the depth in the SEM was more difficult for the finer gratings while the required precision was higher, second, the etch rate and sidewall angle depended more strongly on the groove width as the grooves got narrower. Instead of measuring the depth in between etch steps, dummy samples with nearly identical masks to the real sample were etched first to determine the etch rate and sidewall angle. Because the etch rate also depended on the depth of the groove, at least two dummy samples, etched to different depths close to the desired depth, were required. Once both line width and sidewall angle were known, an optimal depth could be calculated and the sample etched for an appropriate time.

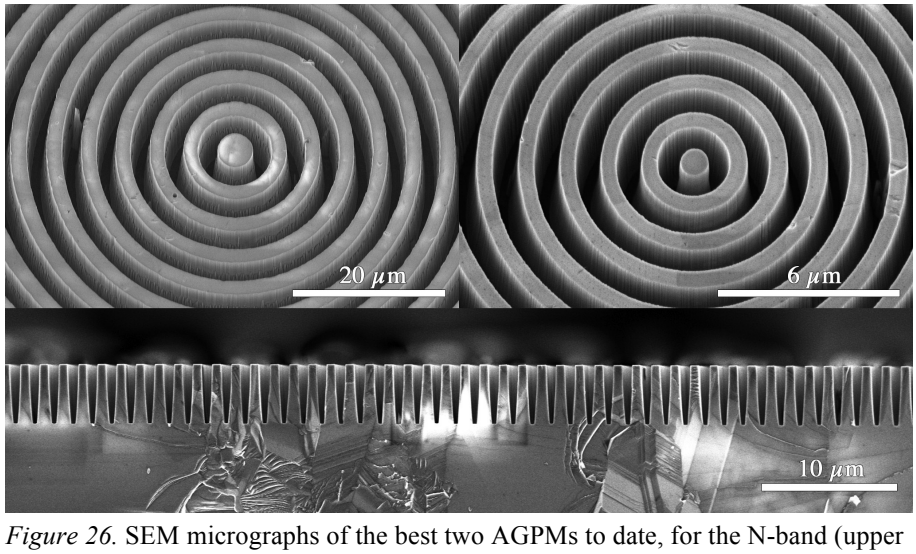

Figure 26. SEM micrographs of the best two AGPMs to date, for the N-band (upper left) and L-band (upper right). At the bottom is a cross section view of a dummy sample cracked in the process of making the L-band AGPM.

Antireflective gratings were etched on the backsides of the AGPM components. This was done to reduce the amount of light reflected inside the com-

ponent, which can give a so-called ghost signal that is not cancelled by the optical vortex.

AGPM performance

The performance of the AGPM components is characterized by the null depth, which corresponds to the ratio between the brightness of a light source as seen through the center of the coronagraph (i.e. with destructive interference) and away from the center (without destructive interference). The grating parameters and calculated null depth, averaged across the spectral band, for our best fabricated AGPMs can be found in Table 1.

Table 1. Grating parameters (as defined in *Figure* 25) and calculated mean null depth for the two best AGPMs.

	Period Λ	**Width w**	**Depth d**	**Angle α.**	**Null depth**
N-band	4.6 µm	1.83 µm	13.8 µm	2.75°	~0.001
L-band	1.42 µm	0.58 µm	5.2 µm	3.1°	~0.001

The null depth presented in Table 1 is calculated for the AGPM alone. To estimate the expected performance of the components, the ghost signal from double reflections in the component should also be added. This signal can be estimated by multiplying the reflectivities of the back and front of the component. These in turn were estimated from the grating parameters and transmission measurements. The antireflective gratings performed well, reducing the backside reflection from 17% down to an average of just 1-2% across the band, with slightly better performance for the N-band than the L-band. The AGPM grating, while not designed to be antireflective, also reduced the reflectivity to around 5-6%. This means the ghost signal for the components should be around 10^{-3} or perhaps as low as $5x10^{-4}$ in the N-band case. This is a small number, but in the same range as the calculated null depth. Adding them together we find that the expected null depth for our components is around 1/500, which is still very good.

The L-band AGPM has been tested at the Observatoire de Meudon in Paris on an optical bench for testing coronagraphs (**paper III**). The measured null depth was very close to the expected 1/500 across the band. This is the best broadband performance demonstrated for a mid-infrared phase mask to date and is very promising for future exoplanet observations. Installation of this component in the LMIRCam instrument at the Large Binocular Telescope in Arizona is being considered.

To reduce the reflection from the AGPM side, an L-band component was also produced using an etch process similar to that used for broadband antireflective gratings in **paper IV**. This gave walls with triangular tops, which should reduce the reflectivity significantly without affecting the achievable

null depth. More work with this etch process is needed to reach a precision on par with that used for the other AGPMs, but even this first component is promising with an expected null depth of $5x10^{-3}$. This component has been installed and tested in NAOS-CONICA (Nasmyth Adaptive Optics System Near-Infrared Imager and Spectrograph) in the Yepun unit telescope at the Very Large Telescope (VLT) in Chile. The first results (which will be published soon) show that the AGPM really does live up to our expectations.

The N-band AGPM works at a too long wavelength for the test bench and so far only preliminary tests have been made with it in the VISIR (VLT Imager and Spectrometer for the mid-InfraRed) instrument in the Melipal unit telescope at the VLT. The early results are promising, but further tests will be needed to show just how good the component is.

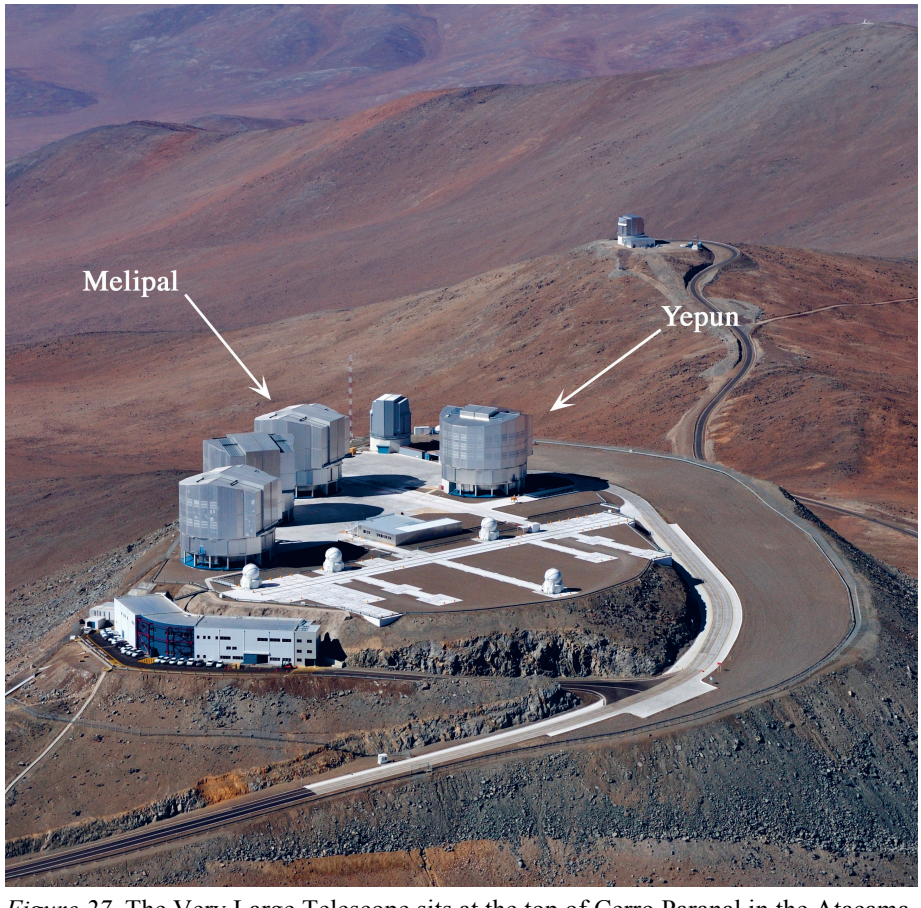

Figure 27. The Very Large Telescope sits at the top of Cerro Paranal in the Atacama desert. Melipal and Yepun are the two unit telescopes where AGPMs have been installed. *Photo by ESO/G.Hüdepohl (atacamaphoto.com)*.

Diamond waveguides for infrared spectroscopy

The angled diamond etching in **paper IV** was developed to allow the etching of smooth beveled ends on a waveguide. Our other uses of it, in etching broadband antireflective gratings and reducing ghost signal in the AGPM, were something of a bonus. The use envisioned for such diamond waveguides is in sensitive infrared spectroscopy using the attenuated total reflectance (ATR) technique.

Attenuated total reflectance

Mid-infrared spectroscopy is a useful method for identifying, quantifying and characterizing many substances, as it utilizes a frequency range that probes vibrations characteristic of the structure of molecules. In standard transmission spectroscopy, the infrared beam is passed through the sample. Light with an energy that corresponds to a resonant frequency in the sample is absorbed giving rise to a spectrum. This is straight forward, but often requires lengthy sample preparation. Solid substances must often be ground and mixed with a salt or oil. A sample of suitable thickness and transparency must then be formed. Quantitative comparisons may be complicated by difficulties in producing homogeneous samples.

In the ATR method, the beam is directed through an IR transparent crystal in contact with the sample instead of through the sample itself. The beam undergoes total internal reflection against the interface between the crystal and the sample (for this the crystal must have a higher refractive index than the sample). Since the electric and magnetic fields can not be discontinuous at the interface, an evanescent wave penetrates a short distance into the sample. This means that energy from the beam can be absorbed by the sample and the spectrum of the beam, after it has passed through the crystal, will be similar to what it would have been if the beam had passed through the sample. The penetration depth of the evanescent wave depends on the wavelength, the refractive indices of the crystal and sample and the angle of the beam. Typically it is around 1/3 of the wavelength. With the ATR technique, the sample can simply be pressed against the crystal (if it is a solid) or a drop can be deposited on it (if it is a liquid).

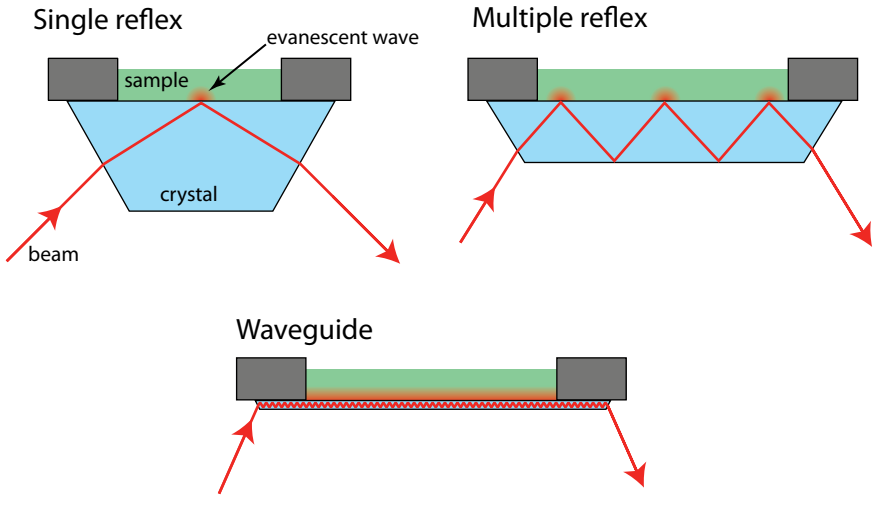

Figure 28. With more reflections, the evanescent path length is increased.

Increasing sensitivity

Multiple reflections – waveguides

To increase the sensitivity of the measurement, multiple reflections of the same beam in the ATR crystal can be used. With each reflection there is an evanescent wave outside the crystal that can interact with the sample and a portion of the light is absorbed, increasing the depth of the bands in the spectrum. In the case of a waveguide the surface area is small, but the number of reflections per unit length is very large, allowing sensitive measurements with very small amounts of sample [38].

Increasing surface concentration

Since the spectrum is only measured for a very thin layer of the sample close to the crystal, sensitivity with a liquid sample can be increased if the molecular species of interest can be made to stay close to the surface instead of moving freely in the solution. One way of doing this is by changing the surface chemistry of the crystal so that the relevant molecules will bind to it. In biological samples it is often of interest to selectively measure a low concentration of a particular protein in a mix of many other proteins and molecules. It is then important not just to bind the interesting proteins to the surface, but also to avoid binding everything else. Binding the wrong sorts of molecules to the surface gives rise to background noise, a lot of signals that are there whether the protein of interest is present or not. If they have similar spectra to what is being measured, it can be difficult or impossible to separate the relevant signal from this noise.

In **paper V** we demonstrate a method of binding a specific protein (in this case C-reactive protein or CRP) to a diamond surface with very little unspecific signal. The basics of this method are as follows (*Figure 29*): The diamond surface is made hydrophobic by hydrogen or fluorine termination (this will be discussed in the section about wetting of diamond surfaces). The central hydrophobic part of a poloxamer adsorbs to the hydrophobic surface. A poloxamer is a copolymer chain with two hydrophilic "arms" connected by a hydrophobic part. The poloxamer used was Pluronic F108 modified with pyridyl disulfide groups at the ends of the arms. Polypeptide binder molecules, specially designed to bind CRP, are attached by reacting with these sulfide groups. The surface is then ready for the sample. CRP molecules in the sample are bound tight to the binder while other proteins find little purchase on the surface. The amount of CRP on the surface was measured by attaching an antibody conjugated with horseradish peroxidase, which could then be detected by chemoluminescence in the presence of luminol and peroxide. For comparison, we performed the same assay on polystyrene and also standard antibody assays on hydrophobic diamond surfaces and polystyrene. The diamond-poloxamer-binder assay gave a very good signal to noise ratio compared with the other assays, allowing lower concentrations of CRP to be detected.

The diamond used in **paper V** is nanocrystalline diamond which would not be suitable for an ATR crystal or waveguide. We did however test the method on a few pieces of high quality microcrystalline diamond and the poloxamer sticks well to that surface as well. The plan is to combine this method of binding molecules to the surface with the speed and increased sensitivity gained from ATR spectroscopy in a waveguide. The waveguides have been produced and we hope to have initial results soon.

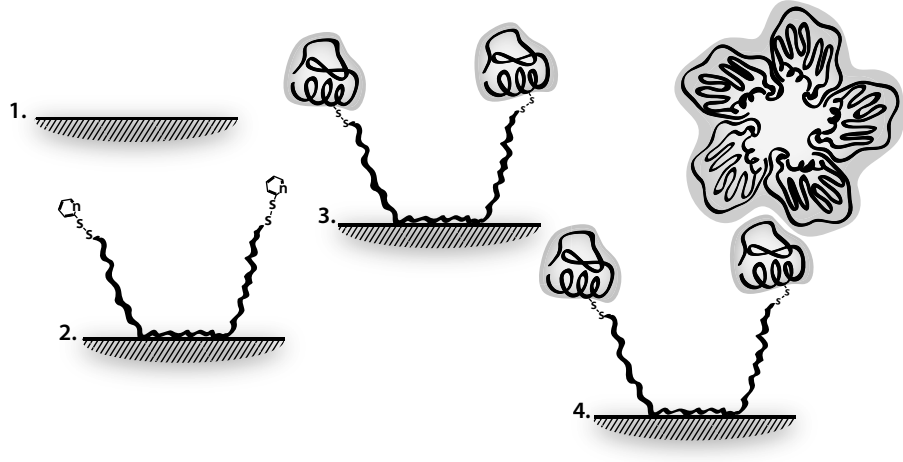

Figure 29. The steps used to bind CRP at a diamond surface: 1. Hydrophobic diamond surface. 2. Pluronic F108-PDS is adsorbed. 3. Designed CRP-binders are attached. 4. The surface can now specifically bind CRP.

Controlling the wettability of diamond surfaces

As we saw in the previous section, there are times when it is important to control the hydrophobicity of a surface. This can be to make molecules stick to it like in **paper V** or the opposite, keeping them off the surface to avoid fouling. Control of hydrophobicity and wetting can be used to separate water from oil, to control how liquid flows in a microchannel or to ensure good contact between an adhesive and a surface for bonding.

Wetting basics

The wetting properties of a surface depend on both its chemistry and its structure. Testing the wettability of a surface is usually done by placing a liquid droplet on it and looking at the three phase contact line, the line where the liquid, solid and vapor phases meet (*Figure 30*).

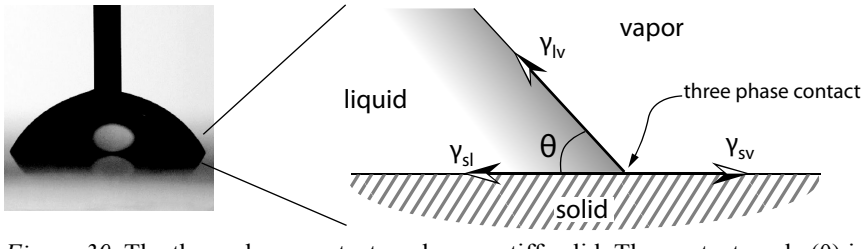

Figure 30. The three phase contact angle on a stiff solid. The contact angle (θ) is measured in the liquid phase between the solid-liquid and liquid-vapor interfaces. γ_{sl}, γ_{lv} and γ_{sv} are the solid-liquid, liquid-vapor and solid-vapor interfacial energies. The droplet on the left has a syringe needle still attached so that the droplet volume can be increased or decreased to measure advancing and receding contact angles.

The contact angle, which is the angle between the solid-liquid and liquid-vapor interfaces, quantifies the wettability on stiff, flat, chemically homogeneous surfaces. On such surfaces, where there are no barriers to reaching thermodynamic equilibrium, the contact angle is determined by a balance between the interfacial energies (or surface tensions) of the three interfaces surrounding the contact line. Balancing the surface tensions horizontally in *Figure 30* gives

$$cos\theta = \frac{\gamma_{sv} - \gamma_{sl}}{\gamma_{lv}}.$$

This is known as Young's equation after Thomas Young. Unfortunately real surfaces are rarely either chemically homogeneous or flat. If the surface is rough, so that the real surface area is larger than the apparent area by a factor *r*, thermodynamic equilibrium yields the Wenzel equation

$$cos\theta_W = rcos\theta_Y.$$

Where θ_W is the macroscopic, measurable contact angle and θ_Y is the contact angle due to surface chemistry. If the surface is instead chemically inhomogeneous with patches of different local contact angles θ_1, θ_2 and so on with corresponding fractions $f_1, f_2, \ldots$ of the surface, the equilibrium contact angle is instead described by Cassie's equation

$$cos\theta_C = f_1 cos\theta_1 + f_2 cos\theta_2 + \cdots$$

On a rough surface with a high inherent contact angle, a liquid may not wet the surface completely but leave pockets of vapor in the deeper parts of the surface. This state can also be described by Cassie's equation if the contact angle on the parts where the liquid rests above air is set to 180°:

$$\begin{aligned} cos\theta_C &= f cos\theta_Y + (1 - f) cos180 \\ &= f cos\theta_Y + f - 1 \end{aligned}$$

where *f* is the fraction of the surface in contact with the liquid. We will call this a Cassie state, while the case where the liquid completely wets a rough surface will be called the Wenzel state. The Cassie state may be metastable, so that the same surface can have droplets in both states depending on how they came to rest on the surface.

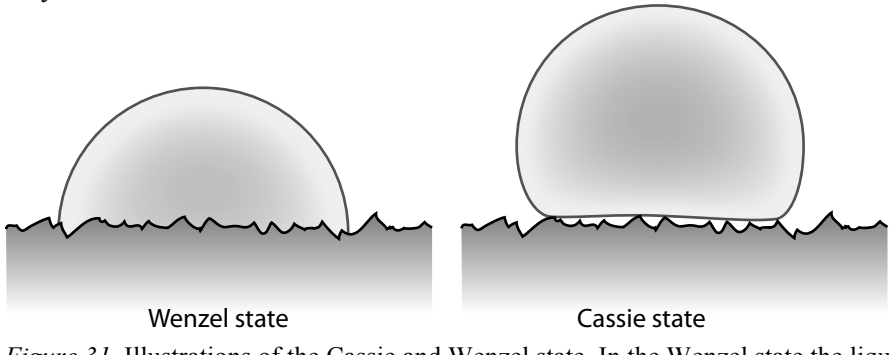

Figure 31. Illustrations of the Cassie and Wenzel state. In the Wenzel state the liquid wets all of the surface under the droplet while in the Cassie state the droplet sits on top of the roughness with pockets of air underneath.

A flat surface can have a contact angle up to ~120° for a fluorinated surface, but as can be seen from Cassie and Wenzel's equations above, higher contact angles can be reached on rough surfaces. In particular if a droplet is resting mostly on air, touching the surface only at the tops of asperities, very high contact angles may be displayed. Such surfaces are often called superhydrophobic (if the liquid is water, which is often the case). The Cassie and Wenzel equations describe a system in thermodynamic equilibrium. On a rough [39] or chemically inhomogeneous [40] surface, there are however free energy barriers that has to be overcome to reach equilibrium. This leads to the observable contact angle taking many different values on the same surface depending on how the contact line moved before coming to rest. This is called contact angle hysteresis. What it leads to in practice is that the equations above only give qualitative predictions and that to characterize the wetting behavior of a liquid on a surface, two contact angles should be measured: The advancing contact angle (θ_a), measured after the contact line has moved toward the dry surface before coming to rest, and the receding contact angle (θ_r), measured after the contact line has withdrawn in the direction of the wet surface. A droplet deposited on the surface with no control can display any contact angle between θ_a and θ_r and does not say much about the wettability of the surface. When both advancing and receding angles are measured however, the surface is well characterized regarding how the liquid will move both when advancing and receding. The amount of hysteresis, $\theta_a - \theta_r$, also says something about the surface and how the liquid rests on it. Large hysteresis values indicate that the surface is rough or chemically inhomogeneous. The Cassie state typically gives smaller hysteresis than the Wenzel state, which can show extreme hysteresis with advancing contact angles of 140° and receding angles of 0° [39].

Measuring contact angles

Measuring contact angles is straightforward. What is needed is a camera-equipped microscope with a long working distance and wide field of view that can be turned horizontally; alternatively a camera with a good macro lens can be used. A way of dispensing small droplets and increasing or reducing their volume is also needed, for our work we have used a purpose built screw actuated syringe with a flat tipped needle. The camera views the droplet from the side, at an angle 1-2° above horizontal. This to ensure that the base of the droplet is visible and that a reflex of the droplet can be seen if the substrate is reflective (which helps with pinpointing the contact line). The droplets should be backlit, with an illuminated white background or diffuse lamp directly behind it. The rest of the background and surroundings of the droplet should be kept dark for good contrast. The set-up is schematically depicted in (*Figure 32*). A droplet is placed on the surface to be studied

with the syringe needle kept in contact with the droplet. Liquid is then injected into the droplet until the contact line is seen to move. After the contact line has come to rest a picture is taken, this will give the advancing contact angle. More liquid is injected and the process is repeated until the droplet volume reaches ~2-4 µl. Liquid is then retracted from the droplet until the contact line can be seen to recede. Again, a picture is taken after the contact line has come to rest to capture the receding contact angle. On superhydrophobic surfaces, the high advancing contact angle can lead to large drop volumes being required before the contact line advances. On such surfaces the droplet can instead be dragged across the substrate by moving the substrate laterally while the syringe and attached droplet are stationary. After stopping a picture can be taken that shows both the advancing and the receding contact angles on opposite sides of the droplet. The contact angles are then measured in the captured pictures. We have used DropSnake, a plug-in for ImageJ developed by the Biomedical Imaging Group at École Polytechnique Fédéral de Lausanne [41].

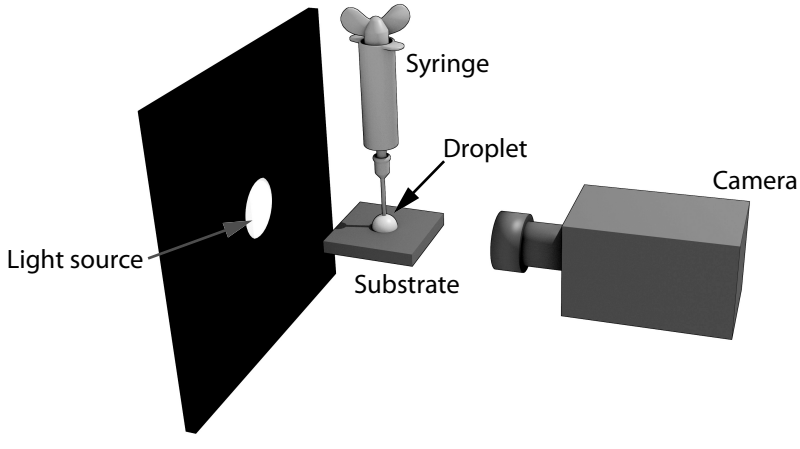

Figure 32. Illustration of the set-up for measuring contact angles.

Wetting on diamond

In **paper VI** we changed the wettability of nanocrystalline diamond (NCD) and microcrystalline diamond (MCD), both by changing the surface chemistry and by etching microstructures.

Diamond termination

At the surface of a diamond crystal, the regular lattice comes to an abrupt end, leaving the carbon atoms at the surface with free bonds to bind some

other species. In the case of CVD diamond, hydrogen is usually abundant during the growth and the as-grown samples end up hydrogen terminated. That is, hydrogen atoms are bound to the carbon atoms at the surface, forming a monolayer. This monolayer can be stripped and replaced with some other species, for example by annealing in a different atmosphere or by plasma treatment. In **papers V and VI** we used heating in a hydrogen atmosphere in a hot filament CVD chamber for hydrogen termination and oxygen and sulfur hexafluoride plasmas for oxygen and fluorine termination respectively. Heating in the presence of atomic hydrogen slowly etched the surface, so the process time for hydrogen termination was kept short ($\lesssim$10 min). The oxygen terminated diamond surfaces were strongly hydrophilic (contact angle close to 0°) while hydrogen and fluorine termination led to more hydrophobic surfaces, fluorine more so than hydrogen. Simulations of diamond surfaces with various terminations show that a pure oxygen termination should actually be hydrophobic (**paper V**), indicating that the oxygen treated surfaces were really mostly OH-terminated. The terminations were confirmed by x-ray photoelectron spectroscopy (XPS), a very sensitive method to determine surface chemistry. Oxygen and Fluorine were measured directly by XPS. Hydrogen could not be measured, so the success of the termination was inferred from contact angle measurements and the absence of other elements at the surface in the XPS measurements. In the spectra from fluorine terminated diamond, the C1s signal was distributed between several distinct binding energies. This indicates that not just CF was present on the surface but also CF_2 and possibly CF_3 [42].

Superhydrophobic diamond surfaces

To produce superhydrophobic diamond samples, 5 μ m square structures were etched in them. Plain pillars were etched in the MCD samples while the NCD was etched into 5 μm square plates, 1 μm thick, resting on narrow silicon stems (*Figure 33*).

The fluorine termination gave high water contact angles on unstructured samples, well above 100°. It was therefore not surprising that all the structured surfaces with this termination were superhydrophobic. Hydrogen termination on the other hand gave advancing contact angles below 90° on unstructured samples. This is too low to maintain a Cassie state on structures with smooth vertical sides; at least 90° is required or capillary forces will pull the liquid down into the surface. As expected, the plain pillar structures on MCD surfaces showed typical Wenzel behavior after hydrogen termination, with moderately low contact angles and large hysteresis.

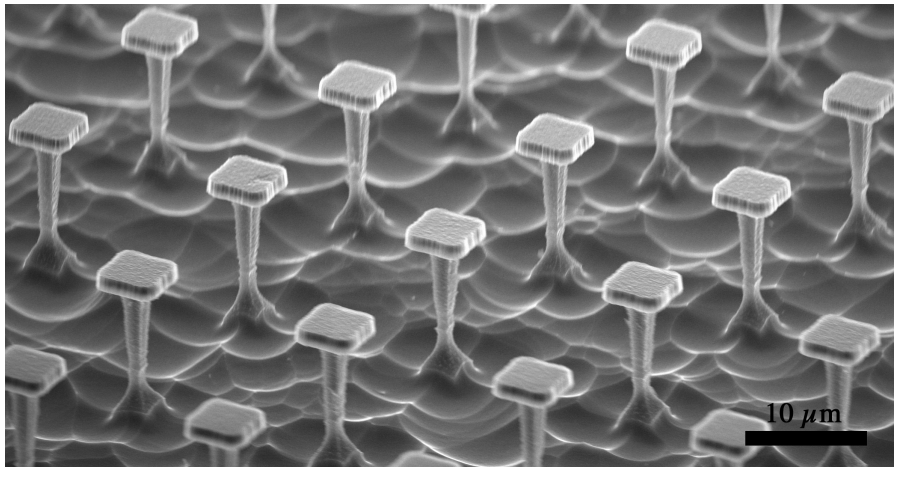

Figure 33. SEM micrograph showing the structure of the superhydrophobic NCD surfaces.

On the NCD samples however, the small diamond disks on silicon stems managed to support a Cassie state. Since the surface consists mostly of moderately hydrophilic silicon, this state is clearly meta-stable. What keeps the water from wetting the silicon stems and reaching the bottom is the shape of the pillar top. To reach an advancing contact angle on the underside of the top plate would require a high curvature of the water surface between pillars (*Figure 34*). Consequently, a high pressure would be needed to push water into the surface. A Cassie state held up in this way is still a fragile thing. If water can reach the bottom in just one place, it can spread through the structure and collapse the whole droplet into the Wenzel state. This was observed when the surface was damaged or the pattern had some defect.

The receding angles measured on the superhydrophobic NCD surfaces with hydrogen termination are curiously low, particularly at high pillar densities. This was probably due to the sides of the top plate being wetted. When receding, the contact line would be pinned by this side before moving from one line of pillars to the next, thereby lowering the measured contact angle.

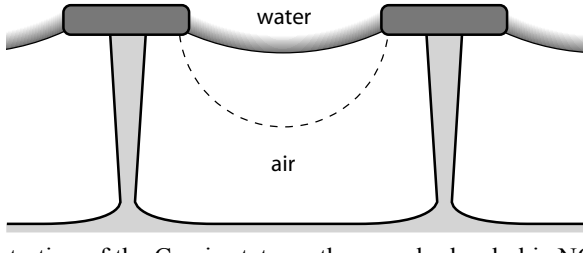

Figure 34. Illustration of the Cassie state on the superhydrophobic NCD surfaces. The dashed line describes the curvature of the water surface necessary to reach the advancing contact angle on the bottom side of the diamond tops.

Superhydrophobic surfaces under pressure

There are many potential uses for superhydrophobic surfaces in microfluidic systems. For one thing, the reduced contact with the solid walls of the channel can reduce the pressure required to push liquid through small capillaries. This reduction of interaction with a solid surface should also reduce problems due to adsorption or fouling. Further, controlling the wettability of different parts of a microfluidic system can direct the liquid flow, this is particularly useful in the case of switchable superhydrophobic surfaces. A superhydrophobic surface also, by its very nature, constitutes an interface between a liquid and a gas phase that may be used to extract or dissolve gasses or trap bubbles. Despite this, not much work has been done on how superhydrophobic surfaces behave under typical conditions one might expect in microfluidics. Such a surface would often be fully submersed so that the air in the surface does not have contact with the outside. It would also be exposed to pressure as channels are filled or liquid is pushed through them. In **paper VII** we investigate how superhydrophobic surfaces consisting of simple pillars behave under pressure. In this paper we show that the pressure required to collapse the Cassie state is increased in an immersed superhydrophobic surface because the pressure in the gas trapped at the surface increases as water is being pushed down into it. We also observed that the Cassie state could be recovered on surfaces with high pillar densities by lowering the water pressure (*Figure 35*). The pillar density required for this in a square array of circular pillars was shown to agree well with a simple comparison of the pressure required to form a bubble on top of the surface with that required for the air-water interface between two diagonally placed pillars to make contact with the next pillar in the water phase.

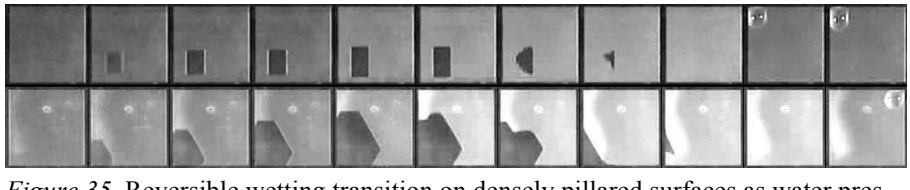

Figure 35. Reversible wetting transition on densely pillared surfaces as water pressure was first increased, then lowered. Top row, square array; bottom row, hexagonal array. As the pressure is increased, the Cassie state collapses in a small area. This area then grows slowly with increasing pressure. When the pressure is lowered sufficiently, the collapsed area shrinks and eventually disappears. Reducing the pressure further causes a bubble to form on the surface.

Diamond microelectrodes

Boron doped diamond is an interesting electrode material for electrochemistry because of its stability and wide potential window in water (the potential difference required to reduce and oxidize water). In **paper VIII** we describe the fabrication and testing of microband electrodes for measurements in a microfluidic channel. The electrodes were an array of 20 µm wide and 500 nm thick stripes, perpendicular to the channel. There were 20 of these electrodes with a separation of 50 µm between them (*Figure 36*). The starting point for the fabrication were silicon wafers with 1 µm silicon oxide and 500 nm heavily boron doped nanocrystalline diamond. The electrodes were relatively large, low aspect ratio structures on a full 4 inch silicon wafer, so patterning with standard UV-lithography and etching with a thin aluminium mask was easily done. The silicon oxide film served both as an insulating layer under the electrodes and as a bonding layer for the PDMS channel. PDMS bonds strongly to silicon oxide after treatment with oxygen plasma and baking, but it does not bond to diamond. The PDMS was clamped firmly to the silicon wafer during bonding to give a tight seal around the electrodes. Fluorescence microscopy was used to confirm that there were no leaks along the electrodes.

The electrodes were tested under rather harsh conditions for several hours with regular electrochemical characterization to confirm their stability. The PDMS channel was then stripped in concentrated sulfuric acid, the electrodes cleaned and a new channel bonded on and tested to demonstrate reusability.

Voltammetry is a sensitive detection method, but it is not very selective. Different substances in the sample may give overlapping signals. The device in **paper VIII** was designed to test electrochemical detection using an external electric field along the microchannel to supply the voltage. The advantage of this approach is that it would be straightforward to integrate such a detection method with capillary electrophoresis and use the same field to drive the separation and supply the potential difference for detection. This has been demonstrated previously using gold electrodes, but they had problems due to oxidation of the adhesion layer needed between gold and silicon oxide [43]. The diamond electrodes on the other hand were extremely stable.

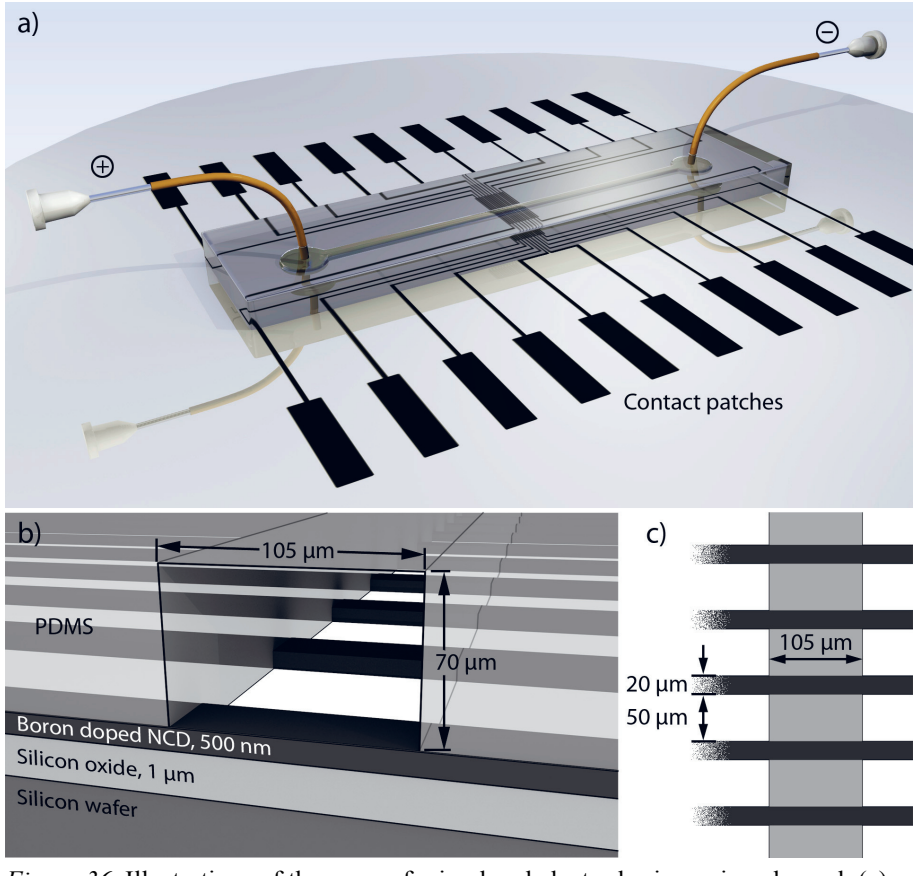

Figure 36. Illustrations of the array of microband electrodes in a microchannel. (a) Overview, (b) cross-section, (c) top view. The set-up is designed to test a concept for using electrochemistry as a detection step after separation by capillary electrophoresis, using the same electric field to drive the separation and supply the voltage for the detection. Figure from **paper VIII**.

Conclusions

The aim of this work has been to improve fabrication methods of diamond microstructures and to demonstrate their utility in a range of applications in optics, sensing and microfluidics. The fabrication improvements made have been in patterning, masking and etching procedures to produce both deep gratings with high precision in all dimensions (**paper I**) and sloped structures (**paper IV**).

The optical applications demonstrated are circularly symmetric half-wave plates for vector vortex coronagraphs in two wavelength bands in the mid infrared (**papers II and III**), broadband antireflective structures for a very wide wavelength regime in the mid to far infrared and smooth angled surfaces for coupling light into and out of waveguides (**paper IV**). The half-wave plates in particular required high aspect ratios and very good precision in all grating parameters (depth, wall width and sidewall angle) in order to perform their optical function. These components have been tested in the lab with good results (**paper III**) and the first results from practical use in a large telescope will be published soon.

A method for controlling the surface chemistry by using Pluronics on hydrophobic diamond surfaces was developed for use in high sensitivity biosensors (**paper V**). Using this surface modification scheme on nanocrystalline diamond surfaces gave very high signal to noise ratios.

Superhydrophobic diamond surfaces were demonstrated using both hydrogen and fluorine terminated diamond (**paper VI**). Hydrogen termination did not make the diamond hydrophobic enough to give rise to superhydrophobicity on pillars with vertical sides, but by controlling the pillar profiles superhydrophobicity could still be achieved. The stability of superhydrophobic surfaces under pressure was also examined (**paper VII**). The collapse of the air film that gives rise to superhydrophobicity was found to be reversible on some densely patterned surfaces when the water pressure was lowered.

Finally, an array of boron doped diamond microelectrodes integrated in a microchannel were fabricated and tested, showing very good stability and reusability (**paper VIII**).

Sammanfattning (Summary in Swedish)

Merparten av världens diamantproduktion går till diverse industriella tillämpningar. I första hand är det diamantens hårdhet som eftertraktas för slipning, borrning, sågning, fräsning och polering. Diamant har dock många andra superlativa egenskaper som gör det till ett intressant material även för mer högteknologiska ändamål. För optik är diamant intressant eftersom det har ett högt brytningsindex och är transparent för nästan alla våglängder från ultraviolett och upp. Goda termiska egenskaper, såsom en extremt hög värmeledningsförmåga och liten värmeutvidgning, gör att diamantoptik lämpar sig särskilt bra för till exempel starka lasrar. Diamant är även kemiskt mycket inert och vävnadskompatibelt vilket gör det intressant för medicinska tillämpningar. Slutligen har diamant även spännande elektriska egenskaper. Det har ett stort bandgap och ren diamant är en god isolator, men dopning med bor eller fosfor kan göra det halvledande. Kraftig bordopning kan dessutom göra diamant till en hygglig ledare. Denna ledningsförmåga i kombination med den kemiska okänsligheten gör bordopad diamant till ett utmärkt material för elektrokemiska elektroder.

Eftersom diamant är så hårt och kemiskt stabilt så är det ett ganska svårt material att forma som man vill. Diamant kan dock etsas med syrgasplasma. Arbetet bakom denna avhandling har syftat till att förbättra metoderna för etsning av mikrostrukturer i diamant samt att demonstrera praktiskt användbara mikrostrukturer. Metodutvecklingen har framför allt rört etsning av djupa gitter och tillverkning av sluttande strukturer i diamant. Det nya i de utvecklade etsmetoderna är i huvudsak användandet av en tjockare etsmask och en bättre kontroll av vinkeln i på maskens kanter. För att tillverka sluttande strukturer etsades masken från kanterna under tiden diamanten etsades på djupet. Användbara strukturer som tillverkats är halvvågsplattor och ytor med låg reflektion för infrarött ljus, vågledare och mikroelektroder för kemisk detektion, samt superhydrofoba diamantytor.

Gitter med en period kortare än ljusets våglängd i materialet (det vill säga kortare än våglängden delad med brytningsindex) har speciella optiska egenskaper. Ljuset beter sig som om ett sådant gitter vore en kontinuerlig film med egenskaper som beror på gittrets form. Genom att designa formen kan man styra brytningsindex och polarisationsegenskaper hos denna ”film”. Detta kräver dock väldigt god noggrannhet i tillverkningsprocessen eftersom små variationer i gittrets form lätt kan påverka dess egenskaper. I den här avhandlingen har tillverkningen av ett flertal sådana subvåglängdsgitter i

diamant beskrivits. En typ av subvåglängdsgitter, som krävt särskilt hög precision, är ett djupt cirkulärt gitter som fungerar som en cirkulärsymmetrisk halvvågsplatta. En sådan halvvågsplatta kan användas som koronagraf, d.v.s. ett instrument i ett teleskop som tillåter observationer av ljussvaga objekt nära en stark ljuskälla. I det här fallet är målet att kunna se planeter kring andra stjärnor. Ett annat subvåglängdsgitter som tillverkats består av höga smala pyramider sida vid sida. Detta gitter kan minska mängden ljus som reflekteras från en diamantyta till en bråkdel över ett mycket stort våglängdsintervall.

Samma metod som användes för att etsa pyramidformer kunde också användas för att tillverka vågledare med släta sluttande ändar. Dessa kan användas för mycket känsliga spektroskopiska mätningar med infrarött ljus. Känsligheten kan förbättras ytterligare genom att kontrollera kemin på ytan så att bara vissa molekyler kan fastna på den. En metod för att göra detta är också beskriven i avhandlingen. Polymerkedjor med en hydrofob (vattenavvisande) mittdel och hydrofila (vattenälskande) ändar fästes på en hydrofob diamantyta. Dessa gör det svårt för andra molekyler att fastna på ytan. Ändarna på kedjorna var modifierade så att designade bindarmolekyler för proteinet CRP kunde fästas där. Den här metoden har än så länge bara använts på plana diamantfilmer och inte på vågledarna, men har redan kunnat mäta mycket små koncentrationer av CRP.

Mikroelektroder i bordopad diamant var relativt lätta att tillverka. De är tänkta att ersätta guldelektroder i ett system för att detektera ämnen separerade med kapillärelektrofores. Guld är ett vanligt elektrodmaterial, men det kräver att man använder en film av en annan metall (ofta krom eller titan) för att fästa på många ytor. Detta är ett problem i elektrokemi då den andra metallen lätt oxideras så att guldelektroderna flagar från ytan. Diamantelektroderna å andra sidan visade sig mycket stabila.

En superhydrofob yta är en yta med en mikrostruktur som kan hålla kvar en luftfilm under vatten. Genom att vattnet vilar mest på luft och bara delvis rör ytan beter sig ytan som helhet som om den vore mer hydrofob än vad som är möjligt för en slät yta. Ett exempel på detta i vardagen är bladen på många växter. De superhydrofoba diamantytorna i denna avhandling var antingen väte- eller fluorterminerade. Väteterminerade diamantytor är normalt inte hydrofoba nog för att ge upphov till superhydrofobicitet, men med en yta bestående av stolpar med en bred topp på ett smalt skaft kan man ändå hålla en luftfilm kvar på ytan.

Acknowledgements

Jag vill tacka en lång rad människor som hjälpt mig på den långa och bitvis krokiga vägen till denna avhandling.

Först och främst vill jag tacka mina handledare. Stort tack Micke för att du varit den bästa handledare jag kunnat önska mig. Tack för att du alltid varit tillgänglig och haft tålamod med mina idéer, såväl bra som dåliga, och för att du kommit med både goda råd och praktisk hjälp i labbet. Det här hade aldrig varit möjligt utan dig. Tack Fredrik för givande samtal och bollande av idéer. Och tack Karin, för en inblick i diamantytors kemi på riktigt liten skala och för att jag fick låna din dator (jag borde kanske lämna tillbaks den nu). Och tack för att du lett diamantcentret och arbetat för att bygga samarbeten kring diamant på Ångströmlaboratoriet.

I also want to thank my previous mentors.

Thank you prof. Niwano for showing me the invaluable combination of a wide-ranging curiosity with a narrow specialization.

Thank you Craig, Rossen, John and Dennis for introducing me to microstructures and to wetting phenomena.

Tack till alla vänner och kollegor på avdelningen, för tips och råd och allmän trevnad i såväl labb som kontors- och fikamiljö. Utan alla udda samtalsämnen på fikarasterna hade de här åren nog känts mycket längre.

Tack till er jag samarbetat med i min forskning.

Eleonora och Leif. Elektrokemi verkade inte så svårt när ni förklarade som jag tror att det egentligen är.

Karin och Lars. Som förstår hur och varför man mäter biomolekyler.

Christian, Olivier, Dimitri, Jean and Serge. For pushing us to push the limits of diamond etching and being there to put the results to good use.

Tack till er på MSL för hjälp med allt i renrummet.

Ett stort tack till min familj som alltid stöttat och uppmuntrat mig, även när jag hållit på med obegripligheter. Jag hoppas den här avhandlingen har visat upp vad jag sysslat med i ett lite klarare ljus.

Tack Pam. Du har hjälpt mer än du vet.

References

[1] Bain & Company, "Diamond Industry Report 2011" (**2011**)

[2] T. M. Babinec, B. J. M. Hausmann, M. Khan, Y. Zhang, J. R. Maze, P. R. Hemmer, and M. Lončar, "A diamond nanowire single-photon source", Nature Nanotechnology 5 (**2010**), 195.

[3] Z. Pan, H. Sun, Y. Zhang, and C. Chen, "Harder than Diamond: Superior Indentation Strength of Wurtzite BN and Lonsdaleite", Physical Review Letters 102 (**2009**), 055503.

[4] T. Irifune, A. Kurio, S. Sakamoto, T. Inoue, and H. Sumiya, "Ultrahard polycrystalline diamond from graphite", Nature 421 (**2003**), 599.

[5] P. J. Heaney, E. P. Vicenzi, and S. De, "Strange Diamonds: The Mysterious Origins of Carbonado and Framesite", Elements 1 (**2005**), 85.

[6] L. Wei, P. K. Kuo, R. L. Thomas, T. R. Anthony, and W. F. Banholzer, "Thermal Conductivity of Isotopically Modified Single Crystal Diamond", Physical Review Letters 70 (**1993**), 3764.

[7] P. John, N. Polwart, C. E. Troupe, and J. I. B. Wilson, "The oxidation of (100) textured diamond", Diamond and Related Materials 11 (**2002**), 861.

[8] C. E. Nebel, B. Rezek, D. Shin, H. Uetsuka, and N. Yang, "Diamond for bio-sensor applications", Journal of Physics D: Applied Physics 40 (**2007**), 6443.

[9] S. E. Haggerty, "Diamond genesis in a multiply-constrained model", Nature 320 (**1986**), 34.

[10] A. Deutsch, V. L. Masaitis, F. Langenhorst, and R. A. F. Grieve, "Popigai, Siberia – well preserved giant impact structure, national treasury, and world's geological heritage", Episodes 23 (**2000**), 3.

[11] U. Ott, "Nanodiamonds in meteorites: properties and astrophysical context", Journal of Achievements in Materials and Manufacturing Engineering 37 (**2009**), 779.

[12] J. Garai, S. E. Haggerty, S. Rekhi, and M. Chance, "Infrared absorption investigations confirm the extraterrestrial origin of carbonado diamonds", The Astrophysical Journal 653 (**2006**), L153.

[13] D. W. Olson, "Diamond (Industrial)" in "Mineral Commodity Summaries 2012", U.S. Geological Survey (**2012**).

[14] D. W. Olson, "Diamond, Industrial" in "2010 Minerals Yearbook", U.S Geological Survey (**2010**).

[15] K. Iakoubovskii, M. V. Baidakova, B. H. Wouters, A. Stesmans, G. J. Adriaenssens, A. Y. Vul, P. J. Grobet, "Structure and defects of detonation synthesis nanodiamond", Diamond and Related Materials 9 (**2000**), 861.

[16] R. S. Balmer et al., “Chemical vapour deposition synthetic diamond: materials, technology and applications”, Journal of Physics: Condensed Matter 21 (**2009**), 364221.
[17] O. A. Williams, “Nanocrystalline diamond”, Diamond and Related Materials 20 (**2011**), 621.
[18] M. Karlsson, Klas Hjort, and F. Nikolajeff, “Transfer of continuous-relief diffractive structures into diamond by use of inductively coupled plasma dry etching”, Optics Letters 26 (**2001**), 1752.
[19] E. K. Chow et al., “Nanodiamond Therapeutic Delivery Agents Mediate Enhanced Chemoresistant Tumor Treatment”, Science Translational Medicine 3 (**2011**), 73ra21.
[20] J. R. Rabeau, A. Stacey, A. Rabeau, S. Prawer, F. Jelezko, I. Mirza, and J. Wrachtrup, “Single Nitrogen Vacancy Centers in Chemical Vapor Deposited Diamond Nanocrystals”, Nano Letters 7 (**2007**), 3433.
[21] I. Langmuir, “Oscillations in ionized gases”, Proceedings of the National Academy of Sciences of the United States of America 14 (**1928**), 627.
[22] J. C. McDonald and G. M. Whitesides, “Poly(dimethylsiloxane) as a Material for Fabricating Microfluidic Devices”, Accounts of Chemical Research 35 (**2002**), 491.
[23] T. J. Whetten, A. A. Armstead, T. A. Grzybowski, and A. L. Ruoff, “Etching of diamond with argon and oxygen ion beams”, Journal of Vacuum Science and Technology A 2 (**1984**), 477.
[24] G. S. Sandhu and W. K. Chu, “Reactive ion etching of diamond”, Applied Physics Letters 55 (**1989**), 437.
[25] M. Karlsson and F. Nikolajeff, “Diamond micro-optics: microlenses and antireflection structured surfaces for the infrared spectral region”, Optics Express 11 (**2003**) 502.
[26] D. T. Tran, C. Fansler, T. A. Grotjohn, D. K. Reinhard, and J. Asmussen, “Investigation of mask selectivities and diamond etching using microwave plasma-assisted etching”, Diamond and Related Materials 19 (**2010**), 778.
[27] H. Yoshikawa, S. Shikata, N. Fujimori, N. Sato, and T. Ikehata, “Smooth Surface Dry Etching of Diamond by Very High Frequency Inductively Coupled Plasma”, New Diamond and Frontier Carbon Technology 16 (**2006**), 97.
[28] O. Dorsch, M. Werner, and E. Obermeier, “Dry etching of undoped and boron doped polycrystalline diamond films”, Diamond and Related Materials 4 (**1995**), 456.
[29] T. Yamada, H. Yoshikawa, H. Uetsuka, S. Kumaragurubaran, N. Tokuda, and S. Shikata, “Cycle of two-step etching process using ICP for diamond MEMS applications”, Diamond and Related Materials 16 (**2007**), 996.
[30] C. David et al., “Nanofocusing of hard X-ray free electron laser pulses using diamond based Fresnel zone plates”, Scientific Reports 1 (**2011**), 57
[31] G. F. Ding, H. P. Mao, Y. L. Cai, Y. H. Zhang, X. Yao, and X. L. Zhao, “Micromachining of CVD diamond by RIE for MEMS applications”, Diamond and Related Materials 14 (**2005**), 1543.

[32] S. Kiyohara, K. Ayano, T. Abe, and K. Mori, "Micropatterning of Chemical-Vapor-Deposited Diamond Films in Electron Beam Lithography", Japanese Journal of Applied Physics 39 (**2000**), 4532.

[33] S. Chattopadhyay, Y. F. Huang, Y. J. Jen, A. Ganguly, K. H. Chen, and L. C. Chen, "Anti-reflecting and photonic nanostructures", Materials Science and Engineering R 69 (**2010**), 1.

[34] R. Neuhäuser and T. Schmidt, "Direct Imaging of Extra-solar Planets – Homogeneous Comparison of Detected Planets and Candidates" in: R. K. Tyson (Ed.) "Topics in Adaptive Optics", InTech (**2012**), ISBN: 978-953-307-949-3.

[35] P. Kalas et al., "Optical Images of an Exosolar Planet 25 Light-Years from Earth", Science 322 (**2008**), 1345.

[36] C. Marois et al., "Direct Imaging of Multiple Planets Orbiting the Star HR 8799", Science 322 (**2008**), 1348.

[37] D. Mawet et al., "Taking the vector vortex coronagraph to the next level for ground- and space-based exoplanet imaging instruments: review of technology developments in the USA, Japan, and Europe", Proceedings of SPIE 8151 (**2011**), 815108.

[38] S. E. Plunkett, S. Propst, and M. S. Braiman, "Supported planar germanium waveguides for infrared evanescent-wave sensing", Applied Optics 36 (**1997**), 4055.

[39] P. S. H. Forsberg, C. Priest, M. Brinkmann, R. Sedev, and J. Ralston, "Contact Line Pinning on Microstructured Surfaces for Liquids in the Wenzel State", Langmuir 26 (**2010**), 860.

[40] C. Priest, R. Sedev, and J. Ralston, "Asymmetric Wetting Hysteresis on Chemical Defects", Physical Review Letters 99 (**2007**), 026103.

[41] A. F. Stalder, G. Kulik, D. Sage, L. Barbieri, and P. Hoffmann, "A snake-based approach to accurate determinations of both contact points and contact angles", Colloids and Surfaces A: Physiochemical Engineering Aspects 286 (**2006**), 92.

[42] C. Vivensang, G. Turban, E. Anger, and A. Gicquel, "Reactive ion etching of diamond and diamond-like carbon films", Diamond and Related Materials 3 (**1994**), 645.

[43] O. Ordeig, N. Godino, J. del Campo, F. X. Muñoz, F. Nikolajeff, and L. Nyholm, "On-Chip Electric Field Driven Electrochemical Detection Using a Poly(dimethylsiloxane) Microchannel with Gold Microband Electrodes", Analytical Chemistry 80 (**2008**), 3622.

Acta Universitatis Upsaliensis

Digital Comprehensive Summaries of Uppsala Dissertations from the Faculty of Science and Technology 1015

Editor: The Dean of the Faculty of Science and Technology

A doctoral dissertation from the Faculty of Science and Technology, Uppsala University, is usually a summary of a number of papers. A few copies of the complete dissertation are kept at major Swedish research libraries, while the summary alone is distributed internationally through the series Digital Comprehensive Summaries of Uppsala Dissertations from the Faculty of Science and Technology.

Distribution: publications.uu.se
urn:nbn:se:uu:diva-192567

ACTA
UNIVERSITATIS
UPSALIENSIS
UPPSALA
2013